University of Pennsylvania
ScholarlyCommons

Technical Reports (CIS)

Department of Computer & Information Science

October 1992

Improved Instrumented Compliant Wrist Design

Thomas Lindsay
University of Pennsylvania

Richard P. Paul
University of Pennsylvania

Follow this and additional works at: https://repository.upenn.edu/cis_reports

Recommended Citation

Thomas Lindsay and Richard P. Paul, "Improved Instrumented Compliant Wrist Design", . October 1992.

University of Pennsylvania Department of Computer and Information Science Technical Report No. MS-CIS-92-77.

This paper is posted at ScholarlyCommons. https://repository.upenn.edu/cis_reports/302
For more information, please contact repository@pobox.upenn.edu.

Improved Instrumented Compliant Wrist Design

Abstract

Interaction between robot and environment is an extremely important aspect of robotic research. Compliance helps reduce the impact effects of robot/environment interaction. Hybrid position/force control is important in most robotic tasks; accurate position control is needed in unconstrained directions, and accurate force control is needed in constrained directions. Force control can be more responsive with a compliant force/torque sensor, but positional accuracy is reduced with compliance. An instrumented compliant wrist device can be used to achieve both responsive force control and accurate position control.

The wrist is connect in series between the end of the robot and the tool, and is designed to partially surround the tool, thus reducing the distance between the end of the robot and the end of the tool. The wrist device uses rubber elements for compliance and damping, and a serial linkage, with potentiometers at each joint, is used for sensing the deflections produced in the wrist.

This document describes the newest version of the instrumented compliant wrist, including modifications and improvements to the wrist described in "Design of a Tool Surrounding compliant Instrumented Wrist", available as tech report MS-CIS-91-30, GRASP LAB 258 from the University of Pennsylvania. Changes include a more protective sensing linkage structure and improved electronics. The compliance, kinematics, and accuracy of the wrist are presented. Also, software for determining the wrist transform, and plans for the wrist are given.

Comments

University of Pennsylvania Department of Computer and Information Science Technical Report No. MS-CIS-92-77.

This technical report is available at ScholarlyCommons: https://repository.upenn.edu/cis_reports/302

Improved Instrumented Compliant Wrist Design

MS-CIS-92-77
GRASP LAB 334

Thomas Lindsay
Richard P. Paul

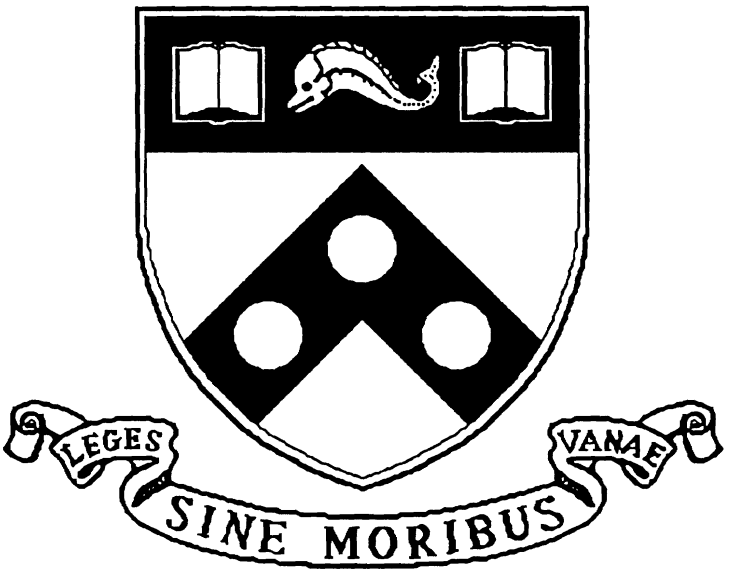

University of Pennsylvania
School of Engineering and Applied Science
Computer and Information Science Department
Philadelphia, PA 19104-6389

October 1992

Improved Instrumented Compliant Wrist Design[†]

Thomas Lindsay and Richard P. Paul

Abstract

Interaction between robot and environment is an extremely important aspect of robotic research. Compliance helps reduce the impact effects of robot/environment interaction. Hybrid position/force control is important in most robotic tasks; accurate position control is needed in unconstrained directions, and accurate force control is needed in constrained directions. Force control can be more responsive with a compliant force/torque sensor, but positional accuracy is reduced with compliance. An instrumented compliant wrist device can be used to achieve both responsive force control and accurate position control.

The wrist is connected in series between the end of the robot and the tool, and is designed to partially surround the tool, thus reducing the distance between the end of the robot and the end of the tool. The wrist device uses rubber elements for compliance and damping, and a serial linkage, with potentiometers at each joint, is used for sensing the deflections produced in the wrist.

This document describes the newest version of the instrumented compliant wrist, including modifications and improvements to the wrist described in "Design of a Tool Surrounding Compliant Instrumented Wrist", available as tech report MS-CIS-91-30, GRASP LAB 258 from the University of Pennsylvania. Changes include a more protective sensing linkage structure and improved electronics. The compliance, kinematics, and accuracy of the wrist are presented. Also, software for determining the wrist transform, and plans for the wrist are given.

[†]This material is based upon work supported by the National Science Foundation under Grant No. BCS-89-01352, "Model-Based Teleoperation in the Presence of Delay." Any opinions, findings, conclusions or recommendations expressed in this publication are those of the authors and do not necessarily reflect the views of the National Science Foundation.

Contents

List of Figures

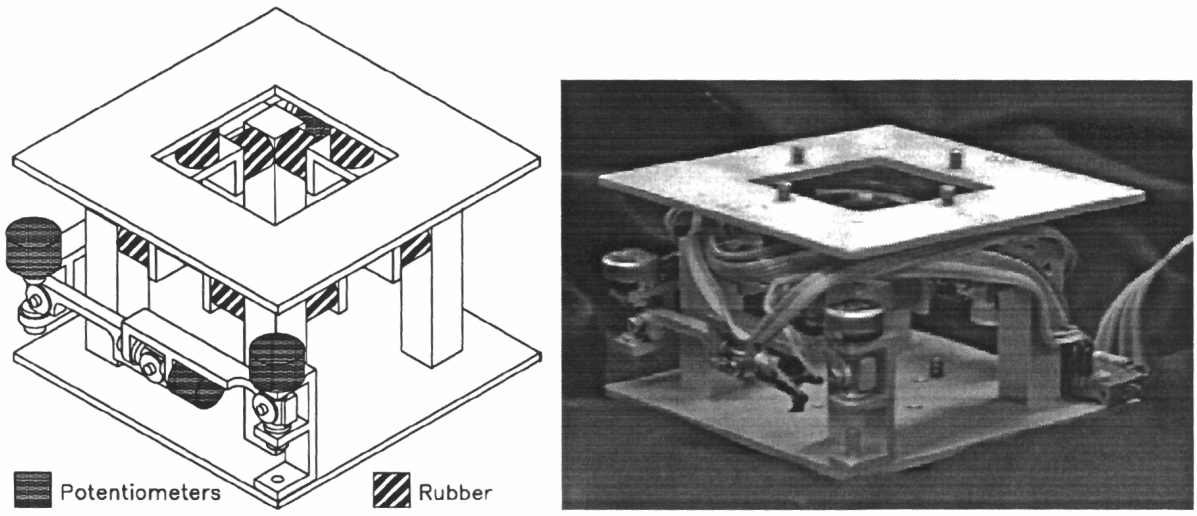

Figure 1: The Tool-Surrounding Instrumented Compliant Wrist

1 Introduction

The wrist outlined herein is a solution to a complex problem: compliance in a robot wrist is desired to reduce the effect of impacts between the robot and the environment, and to create a more responsive force control. However, a compliant wrist by itself limits the effective stiffness of the manipulator in position control, and the exact position of the end of the wrist (and thus the environment, when in contact) is lost [7]. By instrumenting the wrist as described here, both problems are overcome: active control can be used to increase the stiffness of the system, and the position transform of the wrist is sensed. Using the instrumented wrist as a compliant force/torque sensor leads to more responsive force control than with a stiff sensor [5], and more accurate position control than with a compliant wrist [8].

The wrist is overall 4.25 x 4.25 x 3.0 inches high (108 x 108 x76 mm). A 1.75 x 1.75 inch (44.5 x 44.5 mm) tool can be mounted inside the wrist to a depth of 2.5 inches (63.5 mm) maximum, depending on the desired flexure of the wrist.

This report is organized as follows: section 2 outlines the compliance of the wrist, and how it can be modified with different compliant elements, section 3 describes the sensing linkage kinematics, section 4 is a short analysis of the accuracy of the wrist, section 5 contains a simple software routine to compute the wrist transform, section 6 contains the mechanical and electrical plans for the wrist, and section 7 gives a conclusion including current research using the wrist and future work on the wrist.

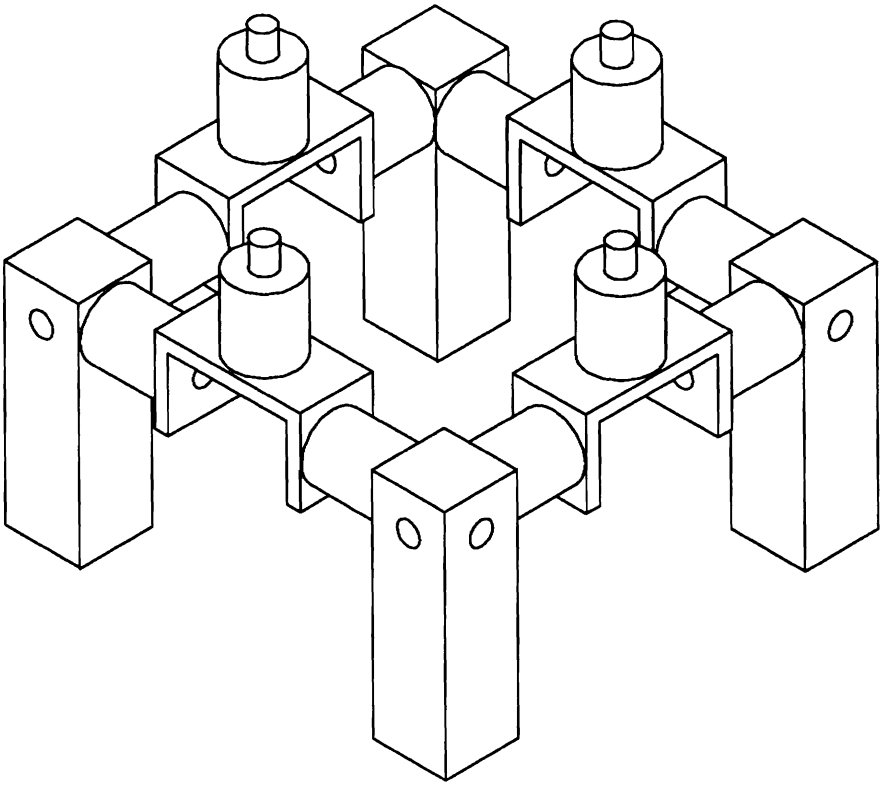

Figure 2: Compliant Structure

2 Compliant Structure

The compliant structure of the wrist is composed of 12 rubber elements, which provide compliance and a small degree of damping. Figure 2 shows the compliant structure design, with the bottom plate (attached to the robot) fixed to the four aluminum blocks at the corners, and the top plate (where the tool is attached) fixed to the four compliant elements (cylinders) at the top. The tool can be partially enclosed in the center of this structure.

The stiffness in each direction can be approximated as follows:

$$K_z = (\frac{1}{4K_a} + \frac{1}{8K_r})^{-1} \tag{1}$$

$$K_x = K_y = (\frac{1}{4K_r} + \frac{1}{4K_a + 4K_r})^{-1} \tag{2}$$

$$K_\psi = (\frac{1}{4K_r L_1^2} + \frac{1}{8K_a L_1^2})^{-1} \tag{3}$$

$$K_\phi = K_\theta = (\frac{1}{2K_a L_1^2} + \frac{1}{4K_r L_1^2 + 4K_r L_2^2})^{-1} \tag{4}$$

where K_a and K_r are the axial and shear stiffnesses of a single element, and L_1 and L_2 are shown in figure 3. This approximation uses the axial and shear stiffness of the rubber elements as supplied by the manufacturer, but ignores any bending stiffness. Age and

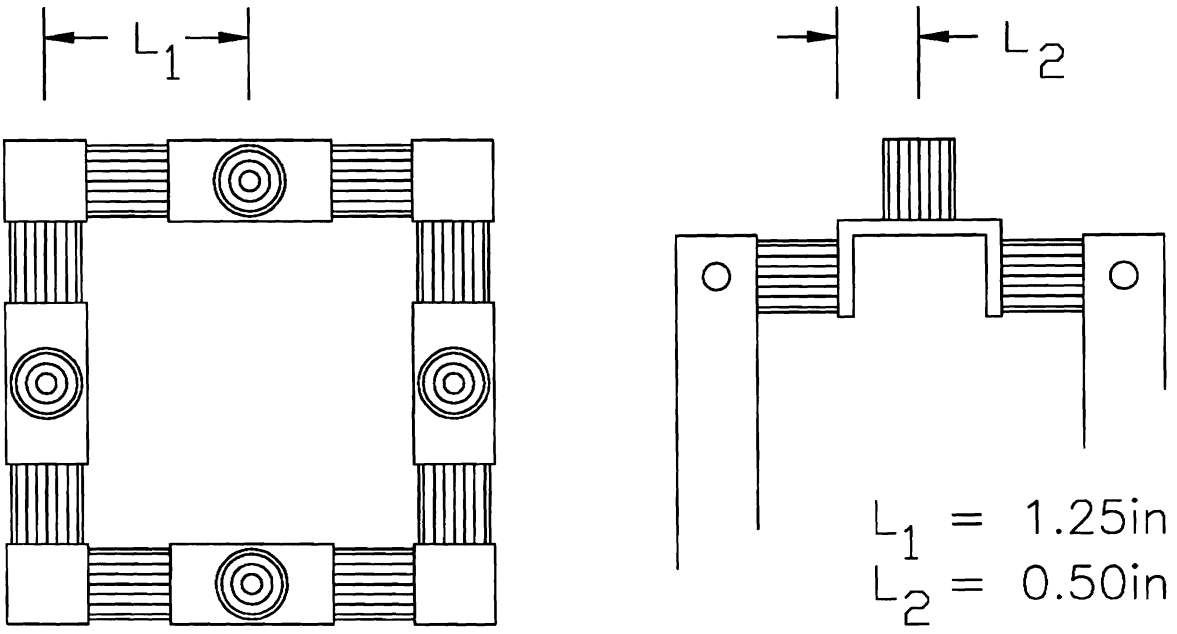

Figure 3: Compliant Structure Measurements

wear for the rubber will also change the stiffness parameters, but this effect has been ignored. For the rubber elements used, the axial stiffness K_a = 66.7 lb/in. (2.63 N/mm) and the shear stiffness K_r = 12.0 lb/in. (.472 N/mm). The approximate compliance of the wrist is tabulated below.

K_x	K_y	K_z	K_ϕ	K_θ	K_ψ
lb/in (N/mm)	lb/in (N/mm)	lb/in (N/mm)	in-lb (N-m)	in-lb (N-m)	in-lb (N-m)
41.65 (7.29)	41.65 (7.29)	70.59 (12.36)	61.37 (6.93)	61.37 (6.93)	68.81 (7.77)

The compliant structure is extremely modular. By exchanging the rubber elements for ones of different properties, the stiffness of the wrist can be changed. For example, the elements can be replaced with any of three similar elements produced by the same manufacturer, or taken away entirely. If the stiffness approximation equations shown above are broken down into individual element stiffnesses, the following equations apply (see figure 4 for element placement numbers):

$$K_z = \left(\frac{1}{(K_{1a}+K_{2a}+K_{3a}+K_{4a})} + \frac{1}{(K_{5r}+K_{6r}+K_{7r}+K_{8r}+K_{9r}+K_{10r}+K_{11r}+K_{12r})}\right)^{-1} \quad (5)$$

$$K_x = \left(\frac{1}{(K_{1r}+K_{2r}+K_{3r}+K_{4r})} + \frac{1}{(K_{7a}+K_{8a}+K_{11a}+K_{12a}+K_{5r}+K_{6r}+K_{9r}+K_{10r})}\right)^{-1} \quad (6)$$

$$K_y = \left(\frac{1}{(K_{1r}+K_{2r}+K_{3r}+K_{4r})} + \frac{1}{(K_{5a}+K_{6a}+K_{9a}+K_{10a}+K_{7r}+K_{8r}+K_{11r}+K_{12r})}\right)^{-1} \quad (7)$$

$$K_\psi = \left(\frac{1}{L_1^2(K_{1r}+K_{2r}+K_{3r}+K_{4r})} + \frac{1}{L_1^2(K_{5a}+K_{6a}+K_{7a}+K_{8a}+K_{9a}+K_{10a}+K_{11a}+K_{12a})}\right)^{-1} \quad (8)$$

$$K_\phi = \left(\frac{1}{L_1^2(K_{2a}+K_{4a})} + \frac{1}{L_1^2(K_{7r}+K_{8r}+K_{11r}+K_{12r})+L_2^2(K_{5r}+K_{6r}+K_{9r}+K_{10r})}\right)^{-1} \quad (9)$$

$$K_\theta = \left(\frac{1}{L_1^2(K_{1a}+K_{3a})} + \frac{1}{L_1^2(K_{5r}+K_{6r}+K_{9r}+K_{10r})+L_2^2(K_{7r}+K_{8r}+K_{11r}+K_{12r})}\right)^{-1} \quad (10)$$

Below is a table of axial and shear stiffness for sample compliant elements. In the current design, mount A is used for all positions on the wrist. Mount n occurs when no mount element is used for a site.

Mount [1]	K_a lb/in (N/mm)	K_r lb/in (N/mm)	comments
A	66.7 (2.63)	12.0 (.472)	mount used
B	92.3	17.6	
C	175.0	37.5	
D	228.6	50.0	
n	0.0	0.0	no mount

Below are some examples of using different elements for the compliant structure.

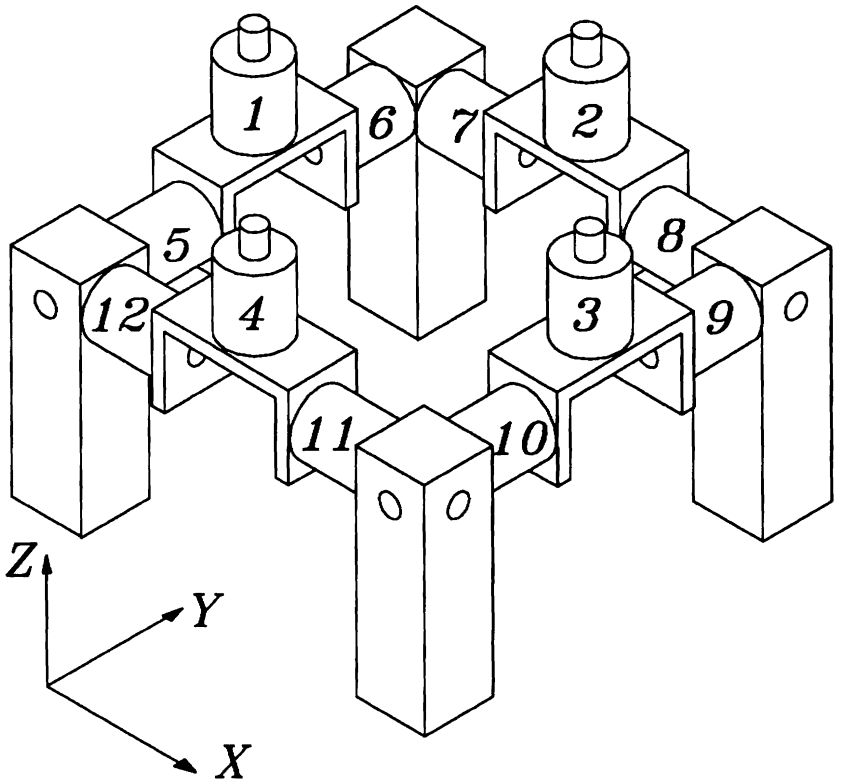

Figure 4: Rubber Element Placement

Element:	1	2	3	4	5	6	7	8	9	10	11	12
Properties:	K_x		K_y		K_z		K_θ		K_ϕ		K_ψ	
Comments	lb/in		lb/in		lb/in		lb-in		lb-in		lb-in	
current	A	A	A	A	A	A	A	A	A	A	A	A
design	41.65		41.65		70.60		61.38		61.38		68.81	
stiffest	D	D	D	D	D	D	D	D	D	D	D	D
	169.57		169.57		278.27		240.47		240.47		281.67	
most	A	A	A	A	A	n	n	A	A	n	n	A
compliant	36.78		36.78		40.68		35.99		35.99		63.56	
stiff in K_z,	A	A	A	A	D	D	D	D	D	D	D	D
K_θ, K_ϕ	46.02		46.02		160.05		132.34		132.34		73.08	
stiff in K_x,	D	D	D	D	A	A	A	A	A	A	A	A
K_y, K_ψ	122.30		122.30		86.88		77.55		77.55		227.30	
compliant	A	A	A	A	A	A	n	n	A	A	n	n
in K_x, K_θ	24.00		40.68		40.68		11.35		66.15		63.56	
even in	B	C	C	B	A	A	A	A	A	A	A	A
trans. dirs.	81.63		81.63		81.39		72.00		72.00		142.71	
even in	A	A	A	A	A	B	B	A	A	B	B	A
rot. dirs.	42.58		42.58		82.01		70.84		70.84		69.74	

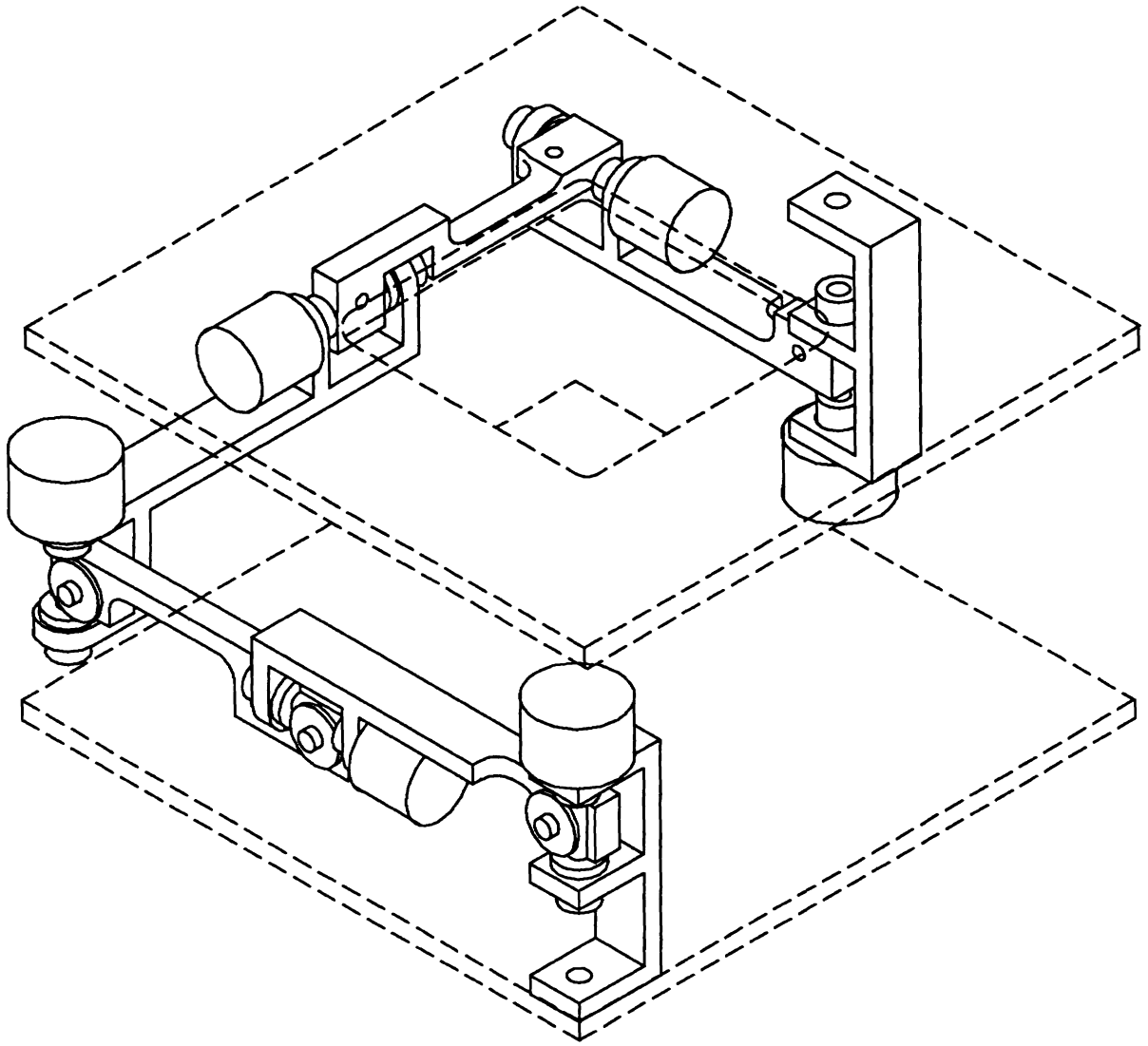

Figure 5: Serial Linkage Chain

3 Linkage Kinematics

The sensing mechanism is composed of a serial linkage chain with potentiometers at each joint (see figure 5). Voltage across the potentiometers is measured to determine the joint angles. Using a simple forward kinematic formulation, the transformation between the robot wrist and the end of the tool can be calculated. The kinematic skeleton of the wrist is shown in figure 6.

The D-H parameters for the sensing linkage mechanism, shown in figures 7 and 8 are:

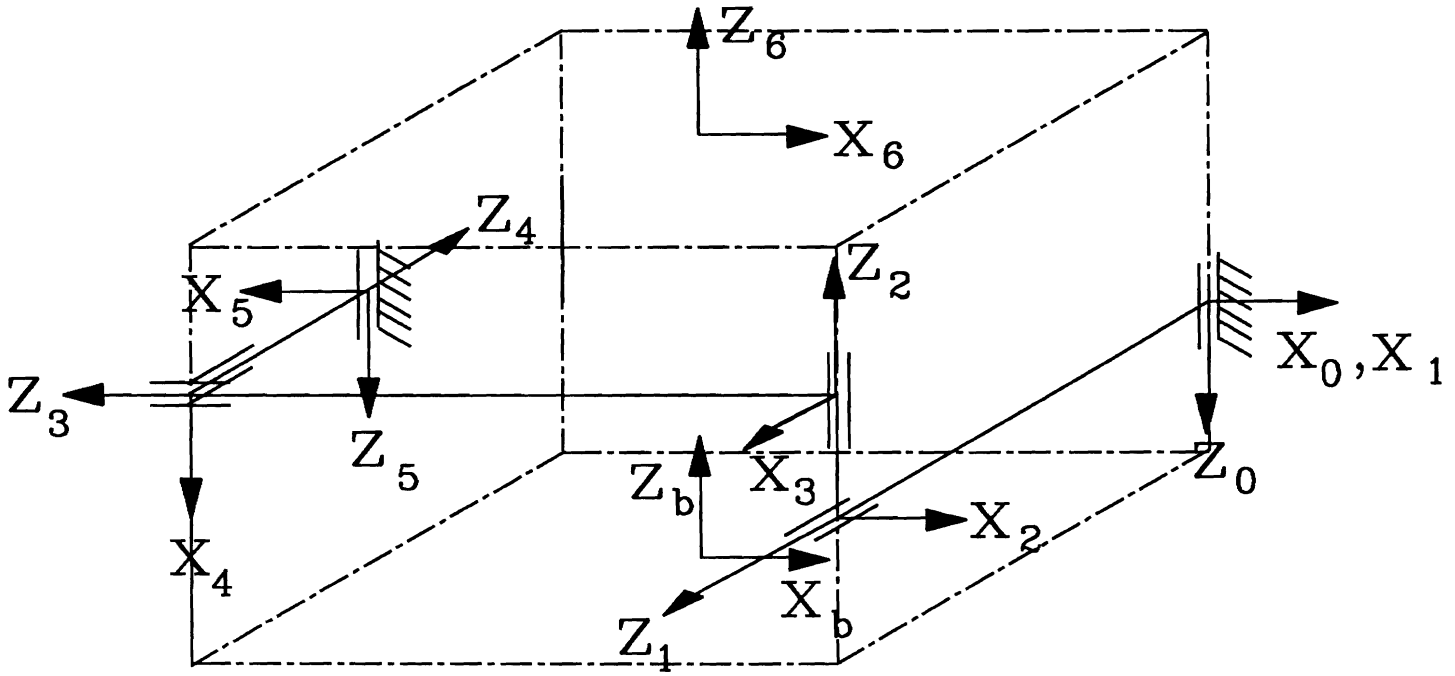

Figure 6: Kinematic Skeleton

joint	a mm	d mm	α deg.	θ deg.
1	0	-25.00	-90	θ_1
2	0	98.82	-90	θ_2
3	0	17.86	90	-90 + θ_3
4	0	98.42	90	-90 + θ_4
5	0	49.61	90	90 + θ_5
6	49.21	-25.00	180	180 + θ_6

Also needed is the transform between the end of the robot (Frame b) and the first link frame:

$$ {}^{b}A_0 = \begin{bmatrix} 1 & 0 & 0 & l_1 \\ 0 & -1 & 0 & l_2 \\ 0 & 0 & -1 & 0 \\ 0 & 0 & 0 & 1 \end{bmatrix} \tag{11} $$

where $l_1 = l_2 = 49.21$mm.

With this information, a transform from the end of the robot to the end of the wrist can be formed. A further transform from the end of the wrist to the end of the tool will complete the transformation from the end of the robot to the tip of the tool.

Relating the $(i-1)$th link frame to the ith link frame is a transform matrix of the form:

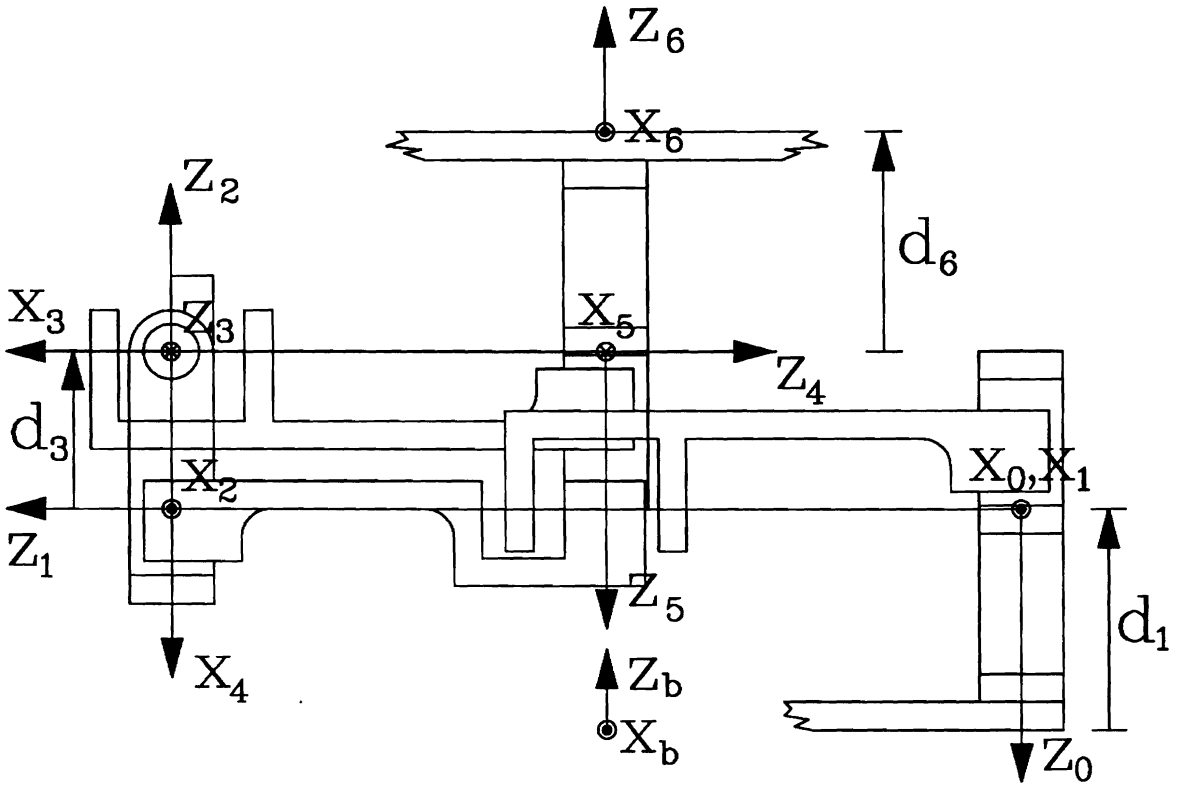

Figure 7: Side view of linkage structure

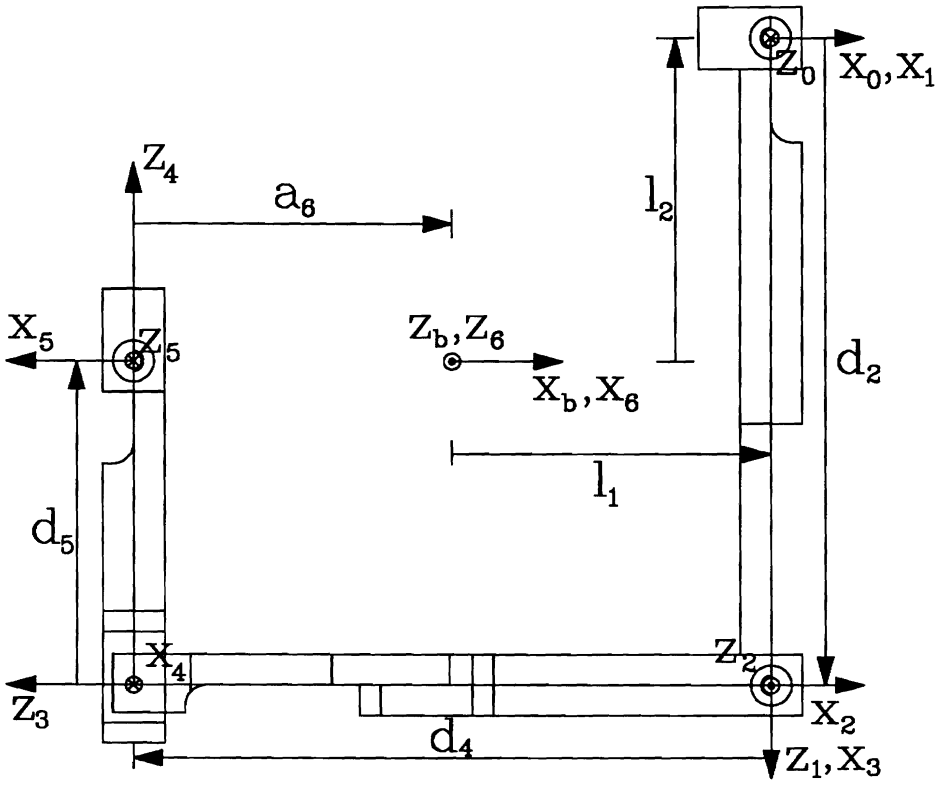

Figure 8: Top view of linkage structure

$$ {}^{i-1}A_i = \begin{bmatrix} \cos\theta_i & -\cos\alpha_i \sin\theta_i & \sin\alpha_i \sin\theta_i & a_i \cos\theta_i \\ \sin\theta_i & \cos\alpha_i \cos\theta_i & -\sin\alpha_i \cos\theta_i & a_i \sin\theta_i \\ 0 & \sin\alpha_i & \cos\alpha_i & d_i \\ 0 & 0 & 0 & 1 \end{bmatrix} \tag{12} $$

The link transforms for the wrist are:

$$ {}^{0}A_1 = \begin{bmatrix} \cos\theta_1 & 0 & -\sin\theta_1 & 0 \\ \sin\theta_1 & 0 & \cos\theta_1 & 0 \\ 0 & -1 & 0 & d_1 \\ 0 & 0 & 0 & 1 \end{bmatrix} \tag{13} $$

$$ {}^{1}A_2 = \begin{bmatrix} \cos\theta_2 & 0 & -\sin\theta_2 & 0 \\ \sin\theta_2 & 0 & \cos\theta_2 & 0 \\ 0 & -1 & 0 & d_2 \\ 0 & 0 & 0 & 1 \end{bmatrix} \tag{14} $$

$$ {}^{2}A_3 = \begin{bmatrix} \sin\theta_3 & 0 & -\cos\theta_3 & 0 \\ -\cos\theta_3 & 0 & -\sin\theta_3 & 0 \\ 0 & 1 & 0 & d_3 \\ 0 & 0 & 0 & 1 \end{bmatrix} \tag{15} $$

$$ {}^{3}A_4 = \begin{bmatrix} \sin\theta_4 & 0 & -\cos\theta_4 & 0 \\ -\cos\theta_4 & 0 & -\sin\theta_4 & 0 \\ 0 & 1 & 0 & d_4 \\ 0 & 0 & 0 & 1 \end{bmatrix} \tag{16} $$

$$ {}^{4}A_5 = \begin{bmatrix} -\sin\theta_5 & 0 & \cos\theta_5 & 0 \\ \cos\theta_5 & 0 & \sin\theta_5 & 0 \\ 0 & 1 & 0 & d_5 \\ 0 & 0 & 0 & 1 \end{bmatrix} \tag{17} $$

$$ {}^{5}A_6 = \begin{bmatrix} -\cos\theta_6 & -\sin\theta_6 & 0 & -a_6\cos\theta_6 \\ -\sin\theta_6 & \cos\theta_6 & 0 & -a_6\sin\theta_6 \\ 0 & 0 & -1 & d_6 \\ 0 & 0 & 0 & 1 \end{bmatrix} \tag{18} $$

Multiplying the A matrices yields ${}^{b}T_6$, the transformation of the wrist.

$$ {}^{b}T_6 = {}^{b}A_0\ {}^{0}A_1\ {}^{1}A_2\ {}^{2}A_3\ {}^{3}A_4\ {}^{4}A_5\ {}^{5}A_6 \tag{19} $$

4 Accuracy

Accuracy of the wrist can be broken into two areas: positional accuracy and hysteresis effects. The positional accuracy is a function of smallest change in position that can be sensed, and sensor noise. The hysteresis effects deal with the ability of the wrist to return to a given position after it has been moved.

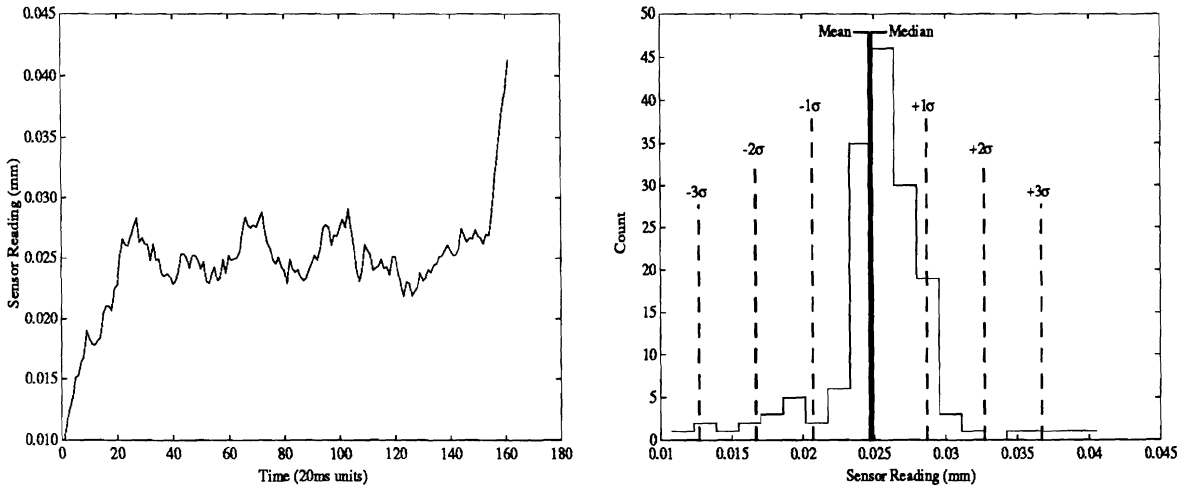

(a) (b)

Figure 9: Sensor Data from Stationary Manipulator

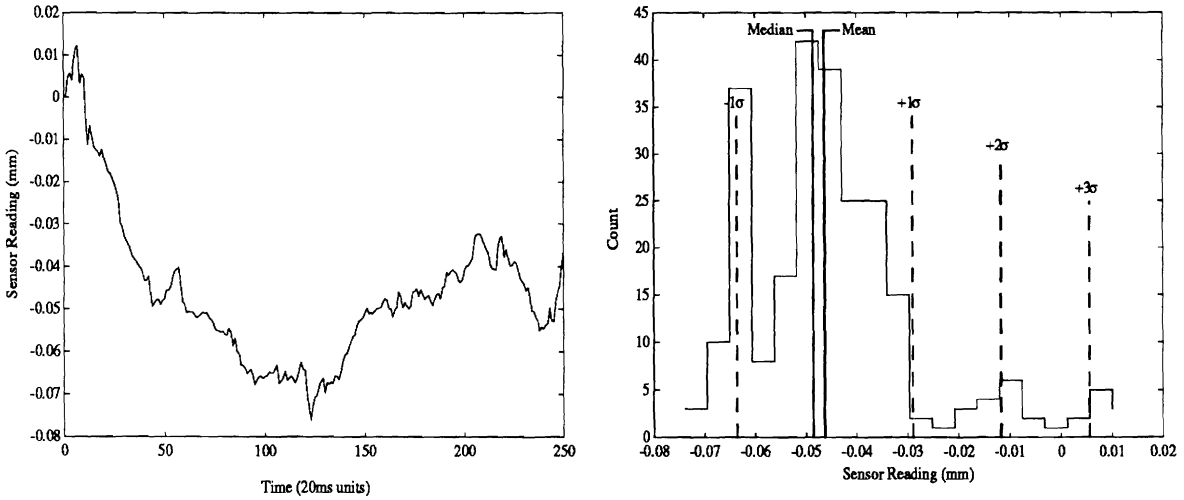

(a) (b)

Figure 10: Sensor Data from Free Space Motion

4.1 Positional Accuracy

The positional accuracy of the wrist is much improved with the addition of a signal conditioner. The potentiometer voltages are differenced from a mid-range reference voltage, and amplified in the signal conditioner board, which is located in close proximity to the wrist itself in order to reduce the effects of line transmission noise. In order to assess the positional accuracy, data from a stationary wrist, free-space motion, and sliding motion (wrist sliding along a flat surface) is presented.

Figure 9 shows sensor data collected when the manipulator is stationary. The fluctuations in sensor data here are caused solely by electrical noise. The actual data is shown in figure 9(a), and the distribution of this data, in histogram format, is shown in 9(b).

Figure 10 shows sensor data from a free-space constant velocity motion, with data collected in the direction of motion. The data fluctuations here are caused by both the electrical noise, as above, and the motion vibrations of the wrist/robot system.

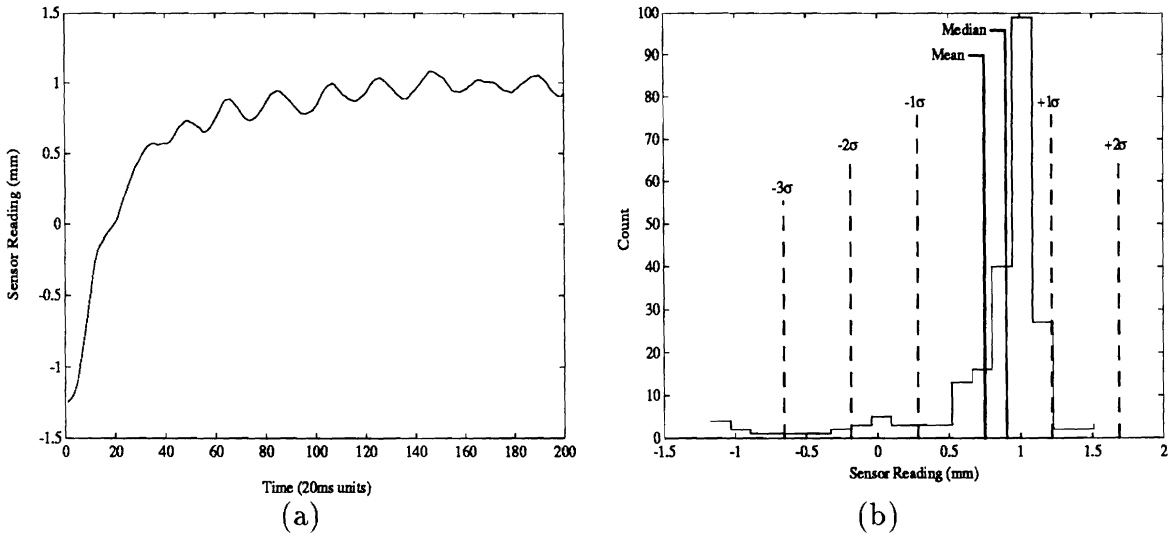

Figure 11: Sensor Data from Sliding Motion

Figure 11 shows sensor data from a sliding motion, while the manipulator is in contact with a surface. Data again is collected in the direction of motion. The fluctuations present in this data result from the electrical and mechanical noise, as above, as well as additional noise associated with the sliding motion. This sliding noise results from:

- Non-ideal control laws which cause the normal force with the surface to fluctuate slightly.
- Non-homogeneous surface friction.
- Coupling of orthogonal forces.

Although data for the sliding motion is highly dependent upon the control laws used for such a motion, it has been presented here as an example of the positional accuracy that may be obtained in a typical application.

Tabulated below are the statistical parameters from the three motions described above.

	mean	median	σ
no motion	0.0247	0.0249	0.0040
free space	-0.0463	-0.0485	0.0173
slide	0.7510	0.9027	0.4685

4.2 Hysteresis Effects

The non-zero mean in the no motion data is an example of the hysteresis effects (data from the wrist in motion is not expected to have a zero mean). Hysteresis effects account for a large portion of the wrist inaccuracy. Factors that contribute to the hysteresis are the natural hysteresis of the rubber compliant elements, which is so small as to be barely noticeable, and effects from friction of the potentiometers coupled with a small amount of bending in the sensing linkage structure.

Tests show that the worst-case inaccuracy due to hysteresis is approximately .6 mm (.025 in.) for translation and .0099 radians (.57 degrees) for rotation. It is clear that this far outweighs the positional inaccuracy.

5 Wrist Software

Below is a listing (in C) for a subroutine to find the wrist transform. Note that in the code, the following are defined:

$$u = {}^{b}A_0\,{}^{0}A_1\,{}^{1}A_2\,{}^{2}A_3\,{}^{3}A_4 \quad (20)$$

$$v = u\,{}^{4}A_5 \quad (21)$$

$${}^{b}T_6 = v\,{}^{5}A_6 \quad (22)$$

```
/*-------------------------------------------------------------------*/
/* WristUpdate(car_diffs)
 *
 *  Reads current angles of wrist sensor and  computes the wrist
 *   transform, also puts the difference of cartesian deflection (from
 *   home position) in the array car_diffs[6]
*/
/*-------------------------------------------------------------------*/

WristUpdate(car_diffs,tw)
float car_diffs[N];
struct transform tw;
{
  float   c1,c2,c3,c4,c5,c6,          /* angle cosines */
  s1,s2,s3,s4,s5,s6,              /* angle sines   */
  u11,u12,u13,u14,u21,u22,u23,u24,u31,u32,u33,u34,
  v11,v12,v13,v14,v21,v22,v23,v24,v31,v32,v33,v34;
  float ang;
  /* Link parameter values */
  float l1 = 49.21, l2 = 49.21;
  float d1 = -25.00,d2 = 98.82,d3 = 17.86,d4 = 98.42,d5=49.61,d6= -25.00;
  float a6 = 49.21;

  ang=rw_jang(0);             /* read joint angle from A/D board */
  c1 = cos(ang);
  s1 = sin(ang);

  ang=rw_jang(1);
  c2 = cos(ang);
  s2 = sin(ang);

  ang=rw_jang(2);
  c3 = cos(ang);
  s3 = sin(ang);
```

```
ang=rw_jang(3);
c4 = cos(ang);
s4 = sin(ang);

ang=rw_jang(4);
c5 = cos(ang);
s5 = sin(ang);

ang=rw_jang(5);
c6 = cos(ang);
s6 = sin(ang);


/* u = A1 * A2 * A3 * A4 */
u11 = c1 * c2 * s3 * s4 - s1 * c3 * s4 + c1 * s2 * c4;
u12 = -c1 * c2 * c3 - s1 * s3;
u13 = -c1 * c2 * s3 * c4 + s1 * c3 * c4 + c1 * s2 * s4;
u14 = -d4 * c1 * c2 * c3 - d4 * s1 * s3
- d3 * c1 * s2 - d2 * s1 + l1;

u21 = -s1 * c2 * s3 * s4 - c1 * c3 * s4 - s1 * s2 * c4;
u22 = s1 * c2 * c3 - c1 * s3;
u23 = s1 * c2 * s3 * c4 + c1 * c3 * c4 - s1 * s2 * s4;
u24 = d4 * s1 * c2 * c3 - d4 * c1 * s3
+ d3 * s1 * s2 - d2 * c1 + l2;

u31 = s2 * s3 * s4 - c2 * c4;
u32 = -s2 * c3;
u33 = -s2 * s3 * c4 - c2 * s4;
u34 = -d4 * s2 * c3 + d3 * c2 - d1;

/* v = u * A5 */
v11 = -u11 * s5 + u12 * c5;
v12 = u13;
v13 = u11 * c5 + u12 * s5;
v14 = d5 * u13 + u14;

v21 = -u21 * s5 + u22 * c5;
v22 = u23;
v23 = u21 * c5 + u22 * s5;
v24 = d5 * u23 + u24;

v31 = -u31 * s5 + u32 * c5;
v32 = u33;
v33 = u31 * c5 + u32 * s5;
v34 = d5 * u33 + u34;
```

```
  /* Wrist transform */
  tw.n.x = -v11 * c6 - v12 * s6;
  tw.o.x = -v11 * s6 + v12 * c6;
  tw.a.x = -v13;
  tw.p.x = -a6 * v11 * c6 - a6 * v12 * s6 + d6 * v13 + v14;

  tw.n.y = -v21 * c6 - v22 * s6;
  tw.o.y = -v21 * s6 + v22 * c6;
  tw.a.y = -v23;
  tw.p.y = -a6 * v21 * c6 - a6 * v22 * s6 + d6 * v23 + v24;

  tw.n.z = -v31 * c6 - v32 * s6;
  tw.o.z = -v31 * s6 + v32 * c6;
  tw.a.z = -v33;
  tw.p.z = -a6 * v31 * c6 - a6 * v32 * s6 + d6 * v33 + v34;

  /* Compute roll, pitch, and yaw angles from wrist transform */
  noatorpy(&car_diffs[5],&car_diffs[4],&car_diffs[3],&tw);
  car_diffs[0] = tw.p.x;
  car_diffs[1] = tw.p.y;
  car_diffs[2] = tw.p.z - 67.86;  /* total wrist thickness */

}

/*-------------------------------------------------------------------*/
```

6 Wrist Plans

6.1 General

The compliant structure and the sensing linkage are sandwiched between the top and bottom plate. The compliant structure is connected to the bottom plate with four 8-32 x 1/2" countersunk machine screws, and to the top plate by the compliant elements. The sensing linkage is attached to the top and bottom plates by two 8-32 x 1/8" countersunk machine screws. The wrist is connected to the robot via a quick mount mechanism (Lord Corporation, not shown), which bolts into the four 8-32 threaded holes in the bottom plate. A 20-pin connector is also attached to the bottom plate.

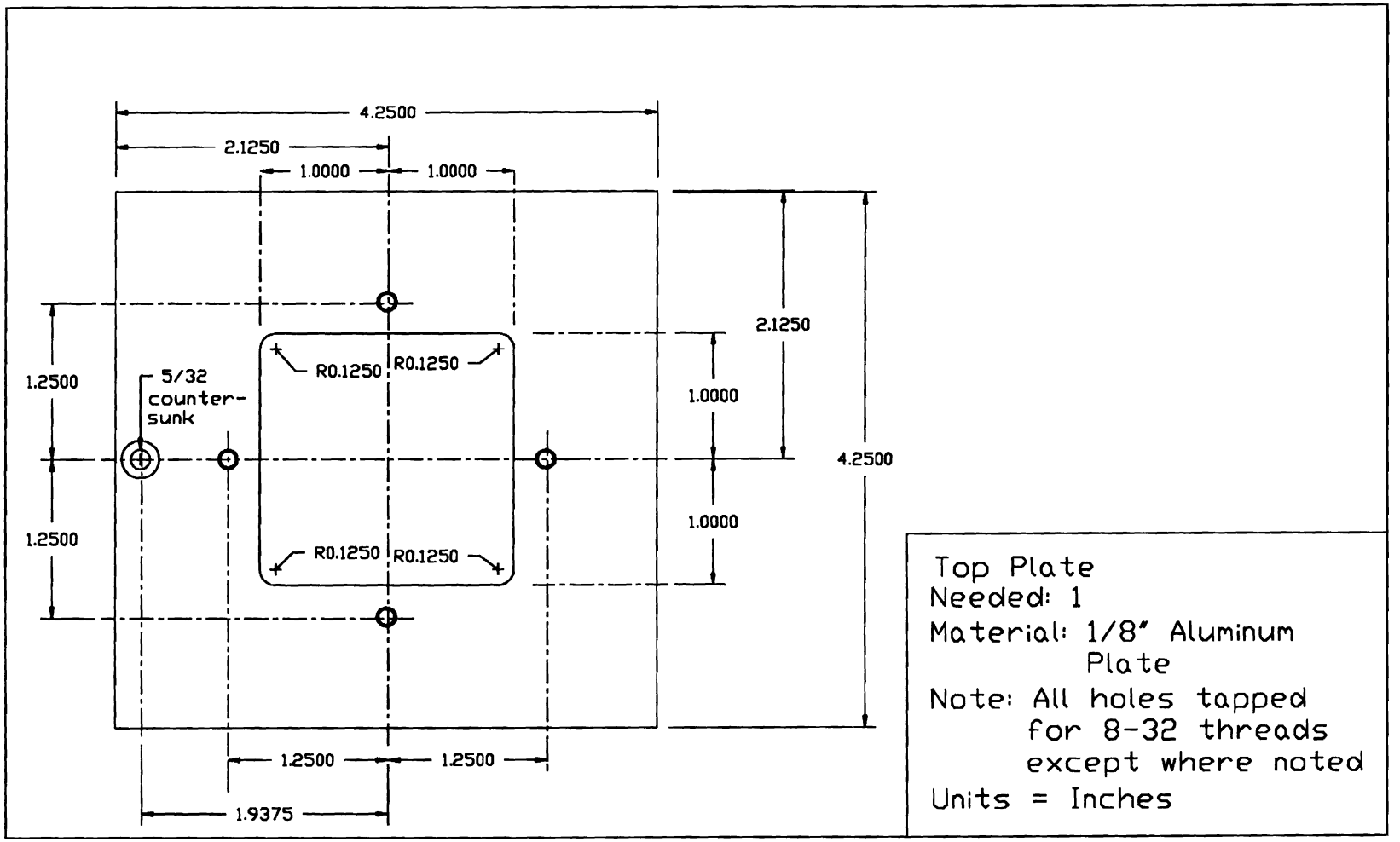

Figure 12: Top Plate

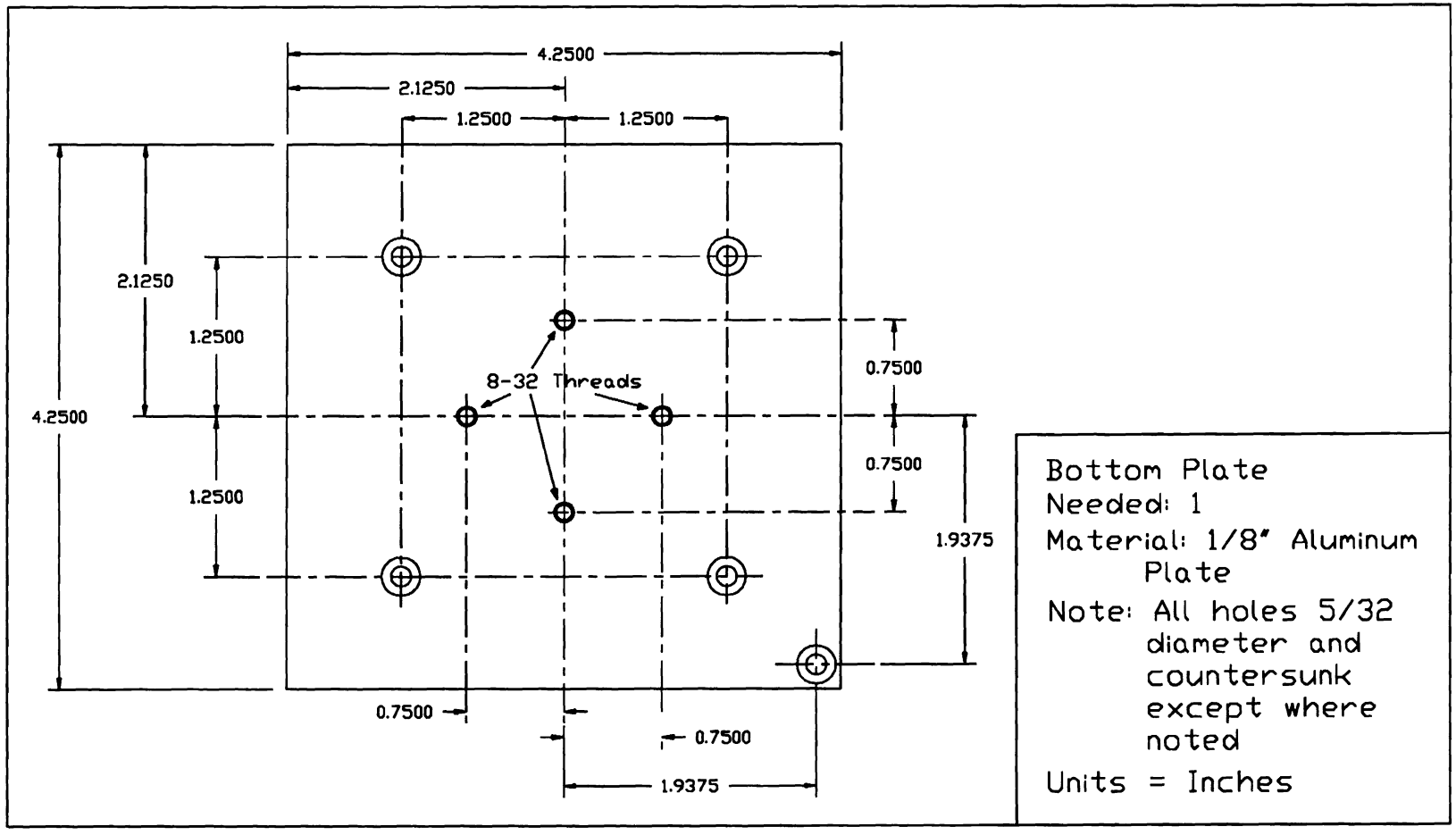

Figure 13: Bottom Plate

6.2 Compliant Structure

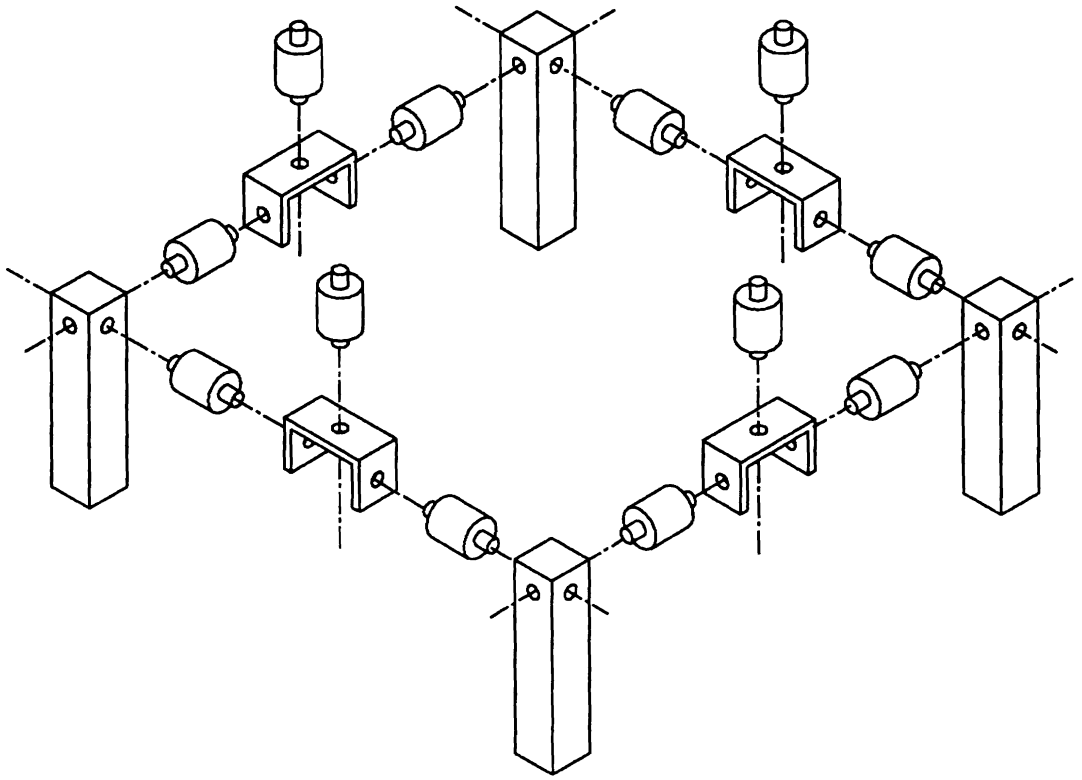

Figure 14: Compliant Structure - Exploded View

The 12 compliant elements are part number 10Z2-302A from Stock Drive Products[1]. These elements have 8-32 x 3/8" threaded studs. Four of these must have one stud shortened to 3/16", one each attached to compliant structure piece 2. All elements connected to compliant structure piece 1 are attached with 8-32 hex nuts.

[1]New Hyde Park, NY, (516) 328-0200. Stiffer elements are part numbers 10Z2-302B, 10Z2-302C, and 10Z2-302D.

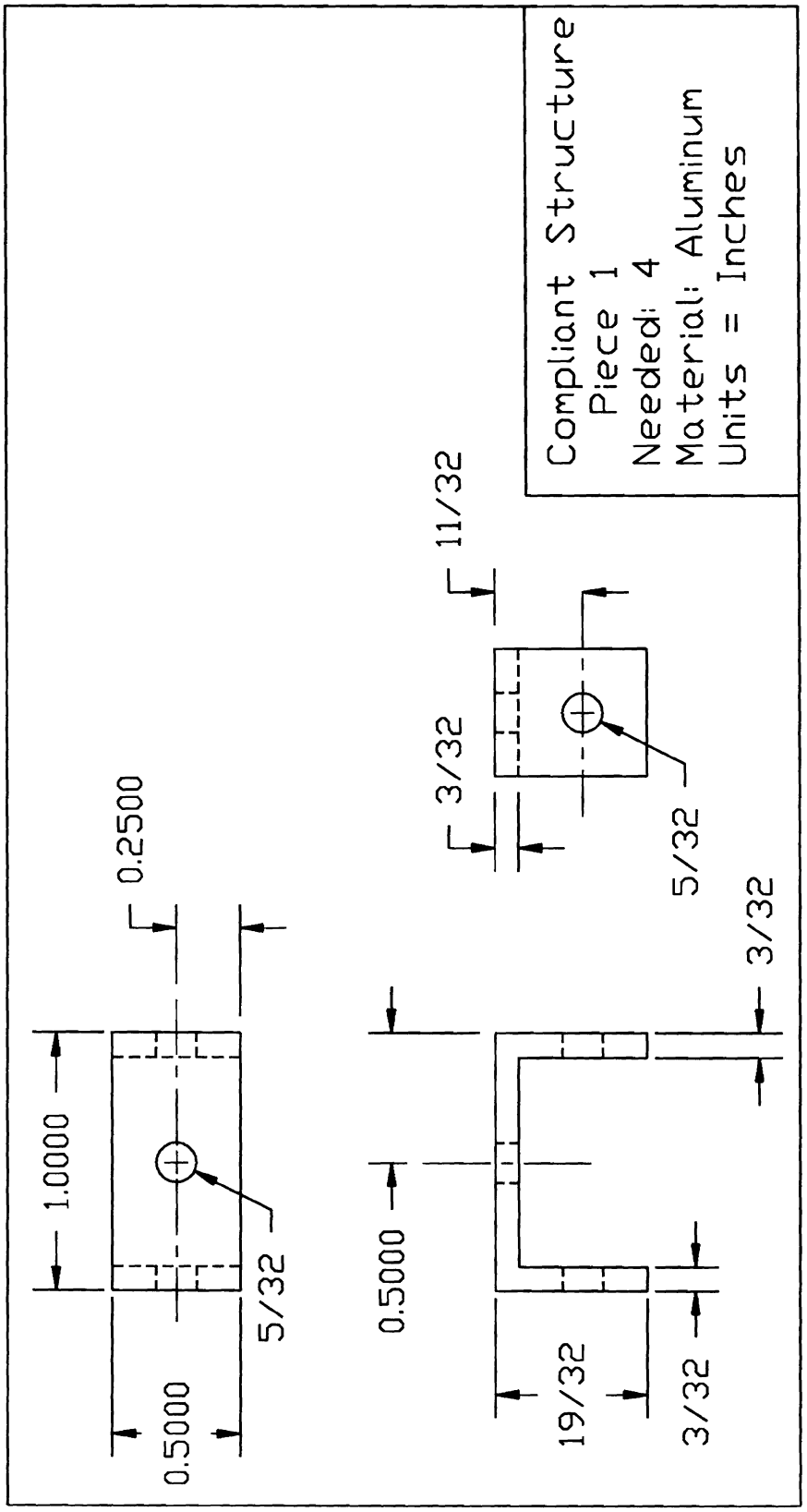

Figure 15: Compliant Structure Piece 1

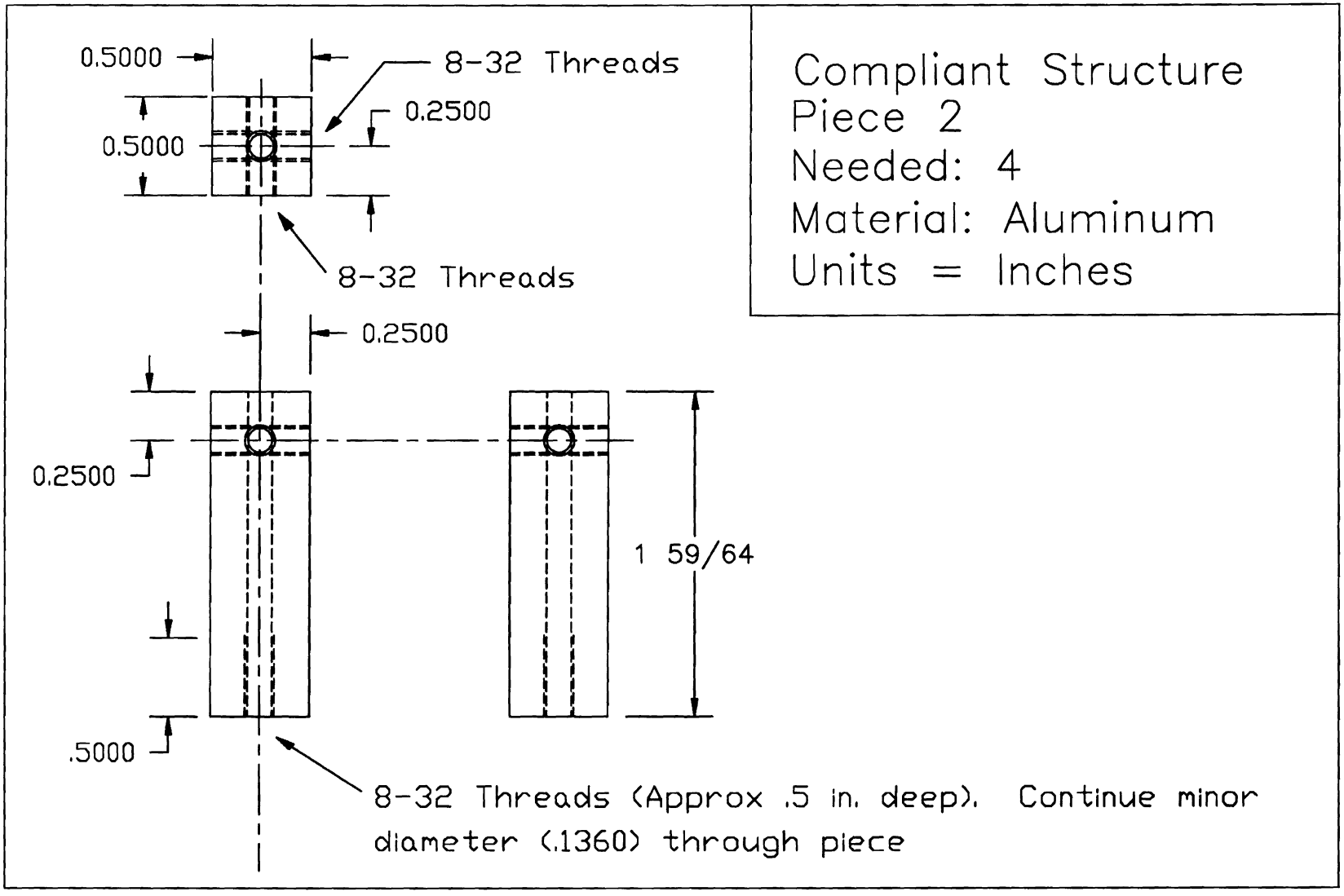

Figure 16: Compliant Structure Piece 2

6.3 Sensing Linkage

Potentiometers used at joints 0, 2, and 5 are part number 381 N 1000 S; joints 1, 3, and 4 are part number RV6 NAYSD 10 2 A from Clarostat Mfg. Co., Inc.[2]. Potentiometers are attached to linkage pieces with 4-40 x 1/4" hex head machine screws and 4-40 flat washers. Each potentiometer has an additional shaft bearing, part number K-FBB-2/4 from Small Parts, Inc.[3]

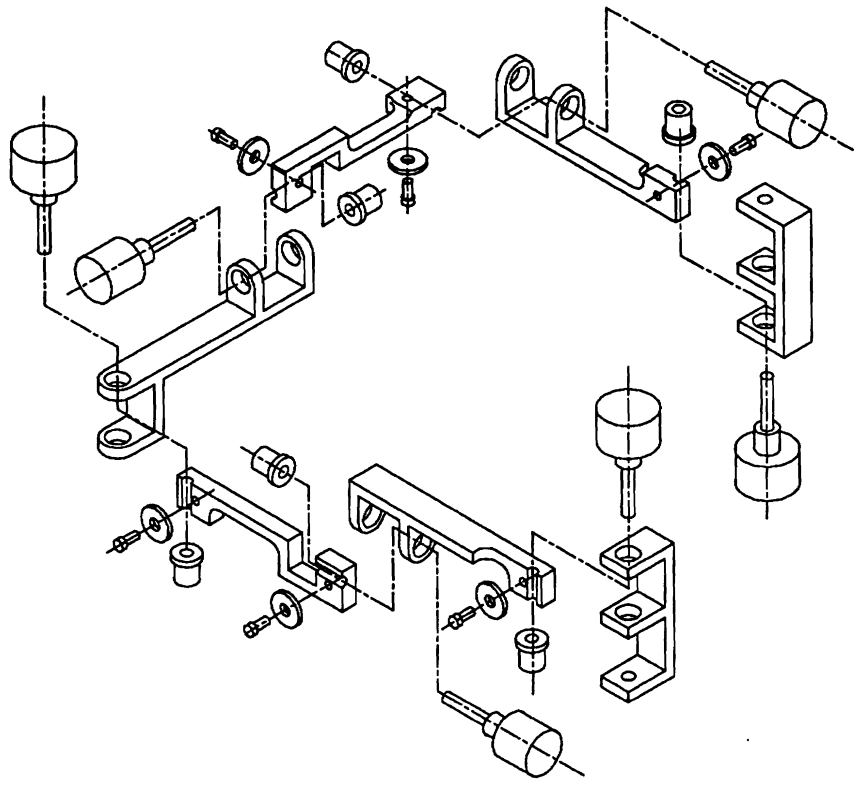

Figure 17: Sensing Linkage - Exploded View

[2]Dover, NH, (800) 872-0042.
[3]Miami Lakes, FL, (305) 557-8222.

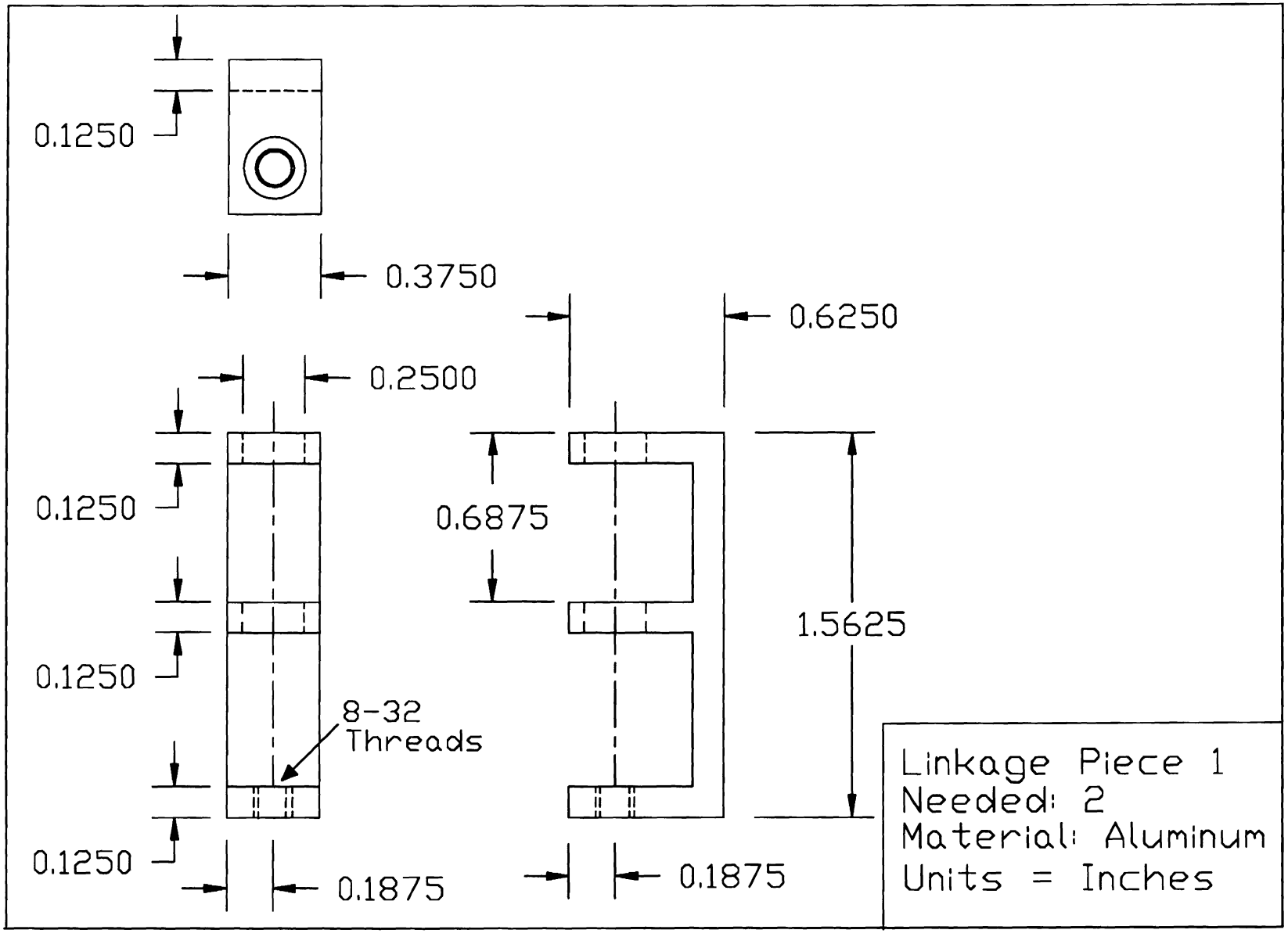

Figure 18: Linkage Piece 1

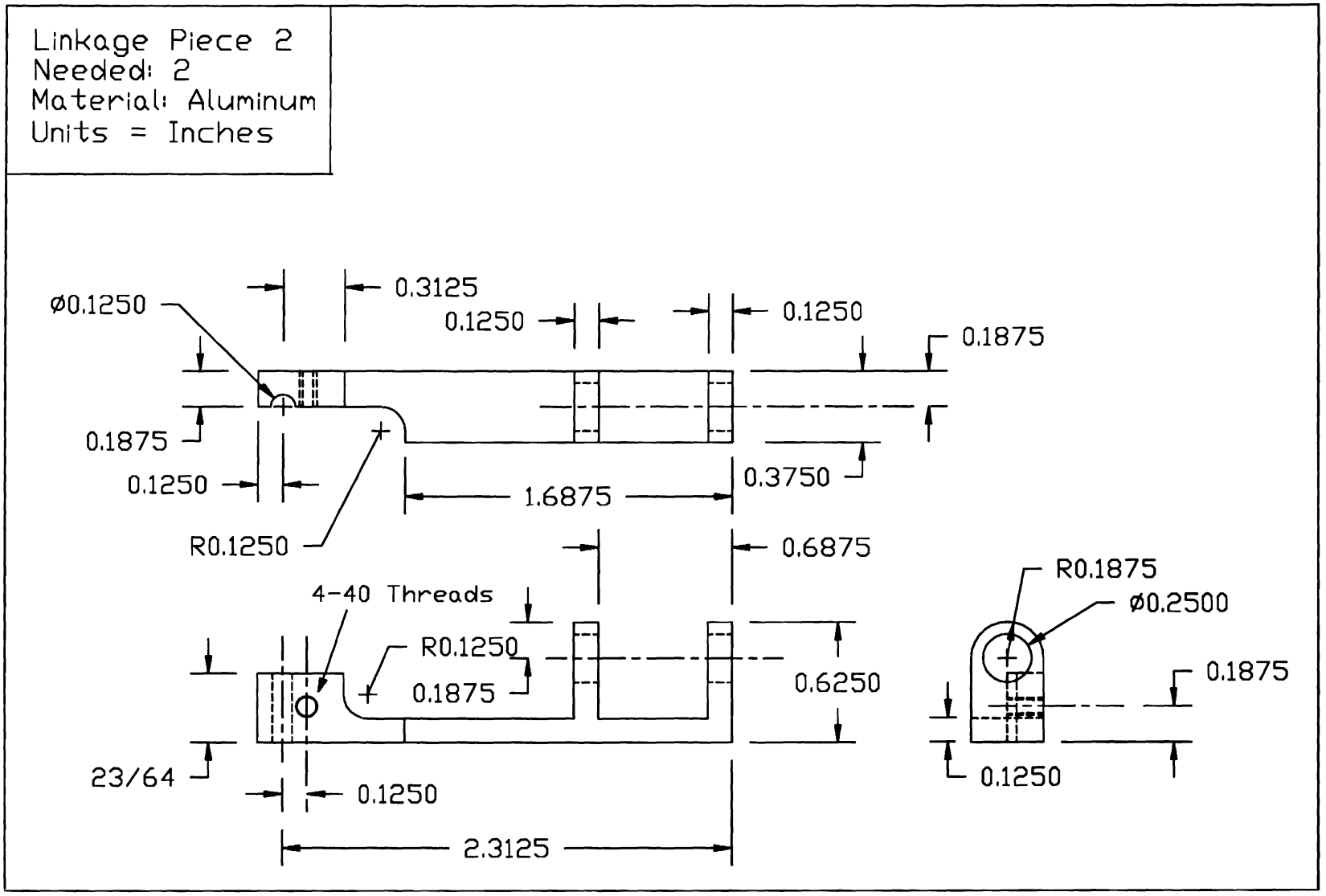

Figure 19: Linkage Piece 2

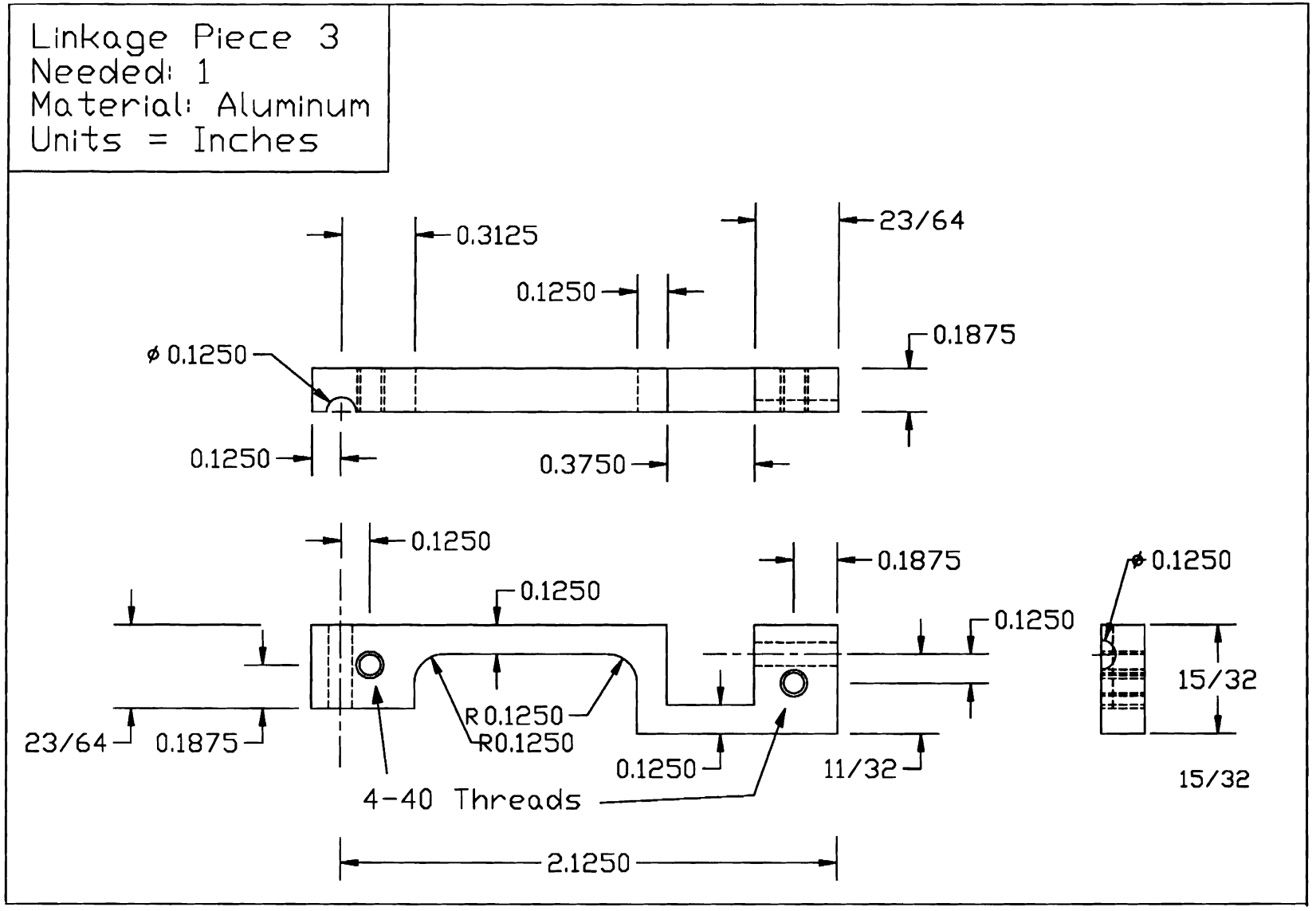

Figure 20: Linkage Piece 3

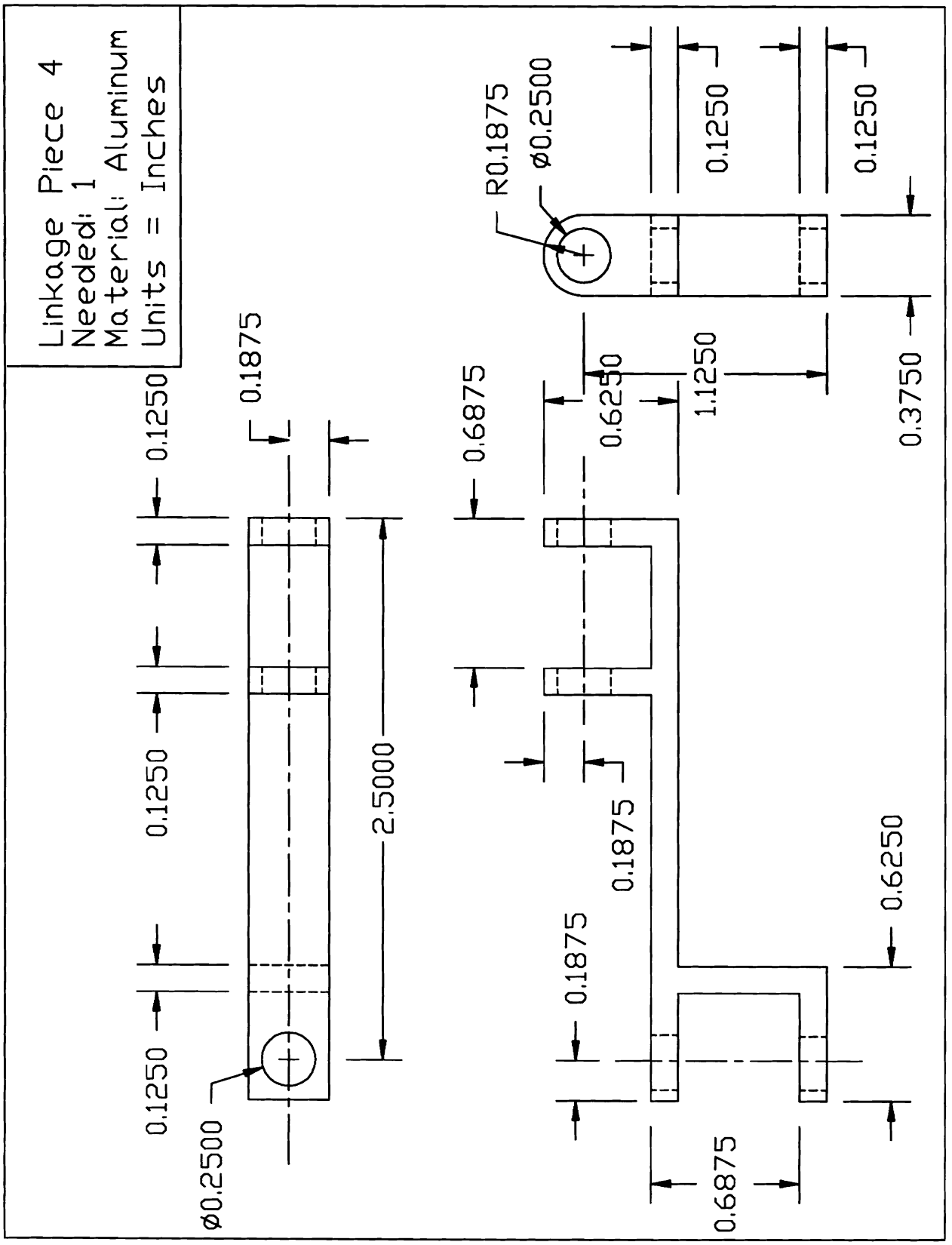

Figure 21: Linkage Piece 4

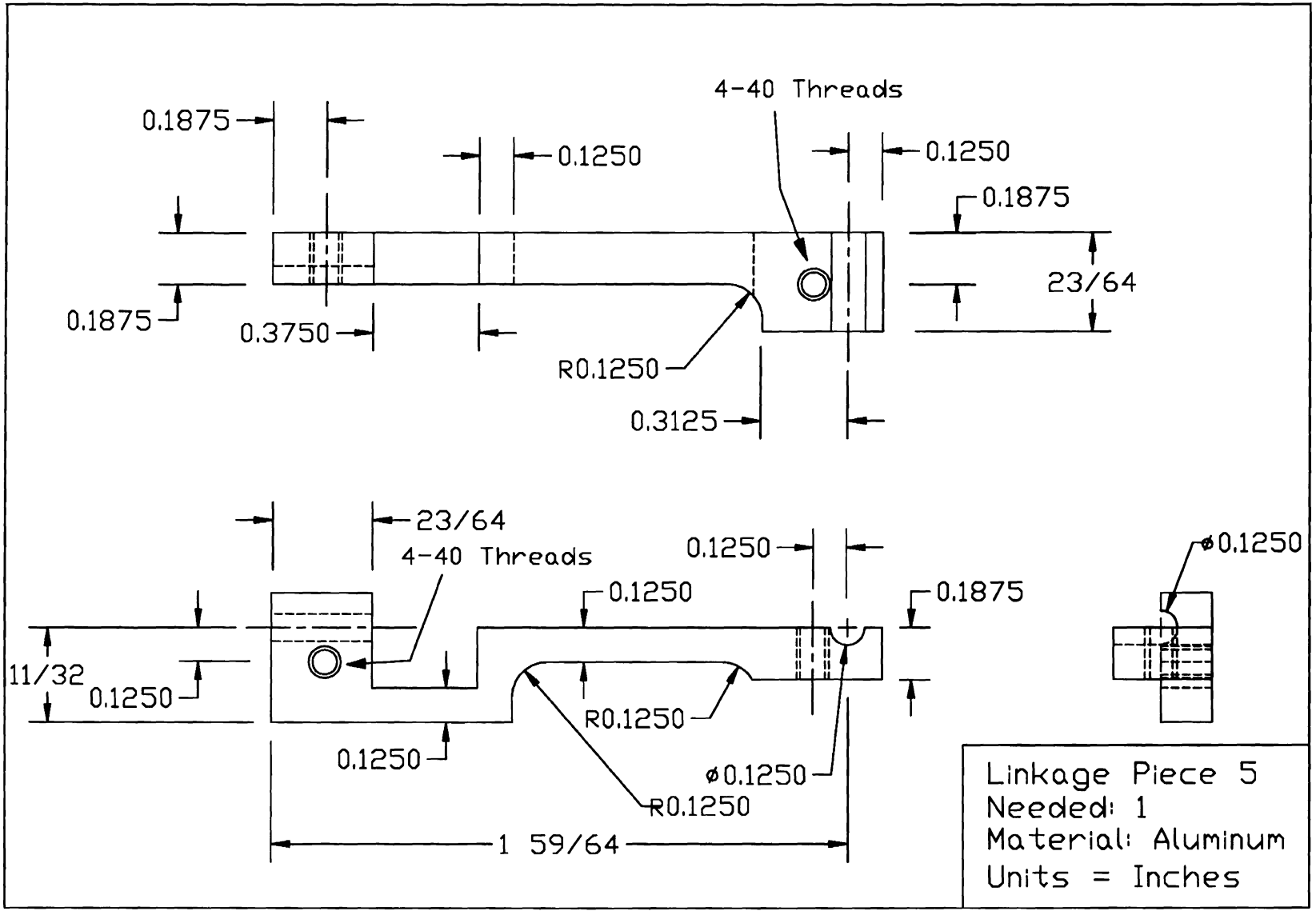

Figure 22: Linkage Piece 5

6.4 Electronics

WRIST CONNECTOR JW1			
SIGNAL NAME	PIN		SIGNAL NAME
P0G	1	2	P0T
P1G	3	4	P1T
P2G	5	6	P2T
P3G	7	8	P3T
P4G	9	10	P4T
P5G	11	12	P5T
P0R	13	14	P1R
P2R	15	16	P3R
P4R	17	18	P5R
WGND	19	20	WGND

JA1					
BOARD	SIGNAL	PIN	PIN	SIGNAL	BOARD
SGND	P0G	1	2	P0T	U1-5
SGND	P1G	3	4	P1T	U2-5
SGND	P2G	5	6	P2T	U3-5
SGND	P3G	7	8	P3T	U4-5
SGND	P4G	9	10	P4T	U5-5
SGND	P5G	11	12	P5T	U6-5
U8-7	P0R	13	14	P1R	U8-7
U8-7	P2R	15	16	P3R	U8-1
U8-1	P4R	17	18	P5R	U8-1
JA2-17	WGND	19	20	WGND	JA2-17

JA2					
BOARD	SIGNAL	PIN	PIN	SIGNAL	BOARD
U1-1	CH0	1	2	RET0	SGND
U2-1	CH1	3	4	RET1	SGND
U3-1	CH2	5	6	RET2	SGND
U4-1	CH3	7	8	RET3	SGND
U5-1	CH4	9	10	RET4	SGND
U6-1	CH5	11	12	RET5	SGND
GND	GND	13	14	GND	GND
-15v	-15v	15	16	-15v	-15v
JA1-19,20	AGND	17	18	GND	GND
+15v	+15v	19	20	+15v	+15v

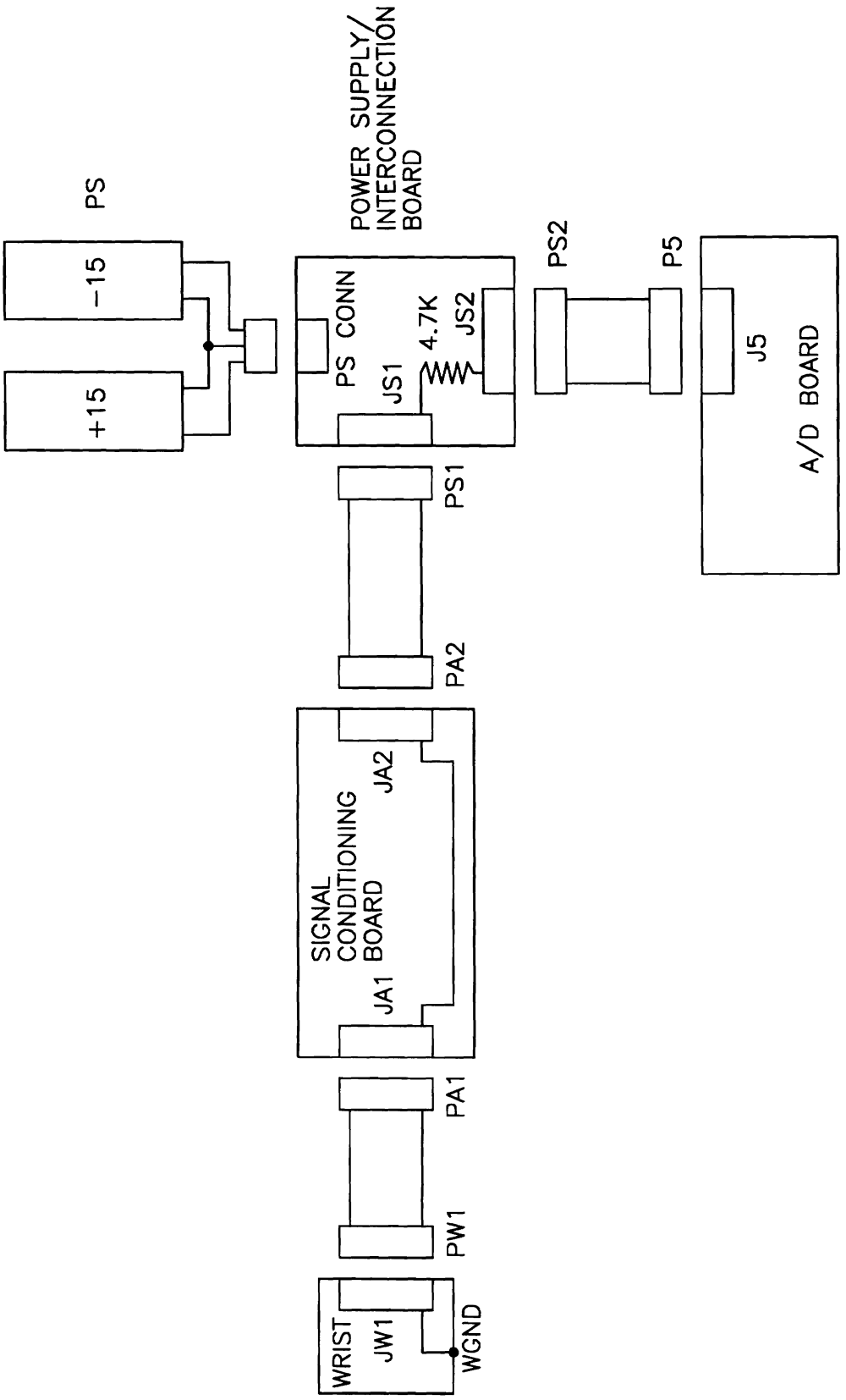

Figure 23: Wrist Power and Connections

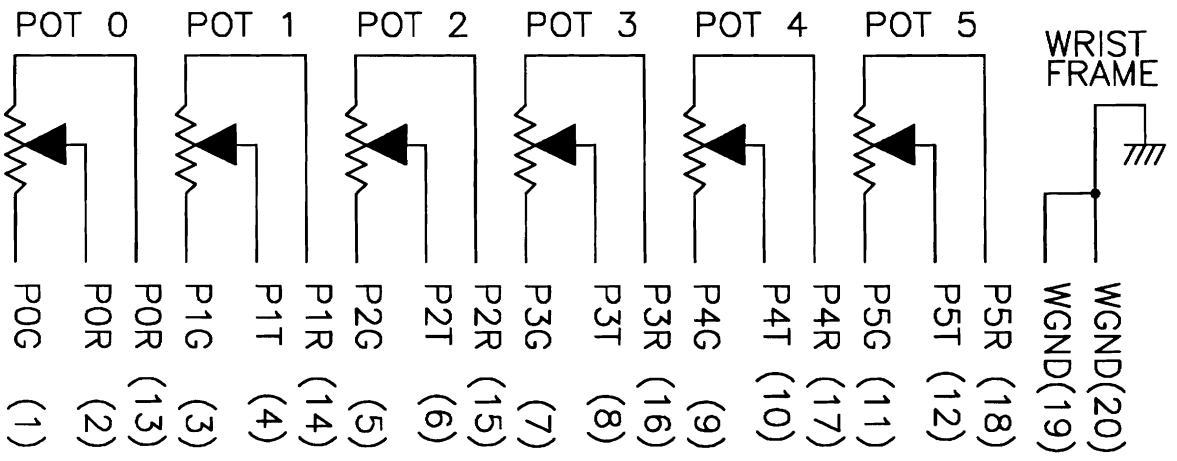

Figure 24: Wrist Electronics

JS1					
BOARD	SIGNAL	PIN	PIN	SIGNAL	BOARD
JS2-1	CH0	1	2	SGND	JS2-18
JS2-3	CH1	3	4	SGND	JS2-18
JS2-5	CH2	5	6	SGND	JS2-18
JS2-7	CH3	7	8	SGND	JS2-18
JS2-9	CH4	9	10	SGND	JS2-18
JS2-11	CH5	11	12	SGND	JS2-18
PS CONN	GND	13	14	GND	PS CONN
PS CONN	-15v	15	16	-15v	PS CONN
JS2-17	AGND	17	18	GND	PS CONN
PS CONN	+15v	19	20	+15v	PS CONN

JS2					
BOARD	SIGNAL	PIN	PIN	SIGNAL	BOARD
JS1-1	CH0	1	2	CH8	JS2-17
JS1-3	CH1	3	4	CH9	JS2-17
JS1-5	CH2	5	6	CH10	JS2-17
JS1-7	CH3	7	8	CH11	JS2-17
JS1-9	CH4	9	10	CH12	JS2-17
JS1-11	CH5	11	12	CH13	JS2-17
JS2-17	CH6	13	14	CH14	JS2-17
JS2-17	CH7	15	16	CH15	JS2-17
JS1-17	AGND	17	18	AMP LO	JS1-2,4,6,8,10,12
N/C	+12v OUT	19	20	-12v OUT	N/C

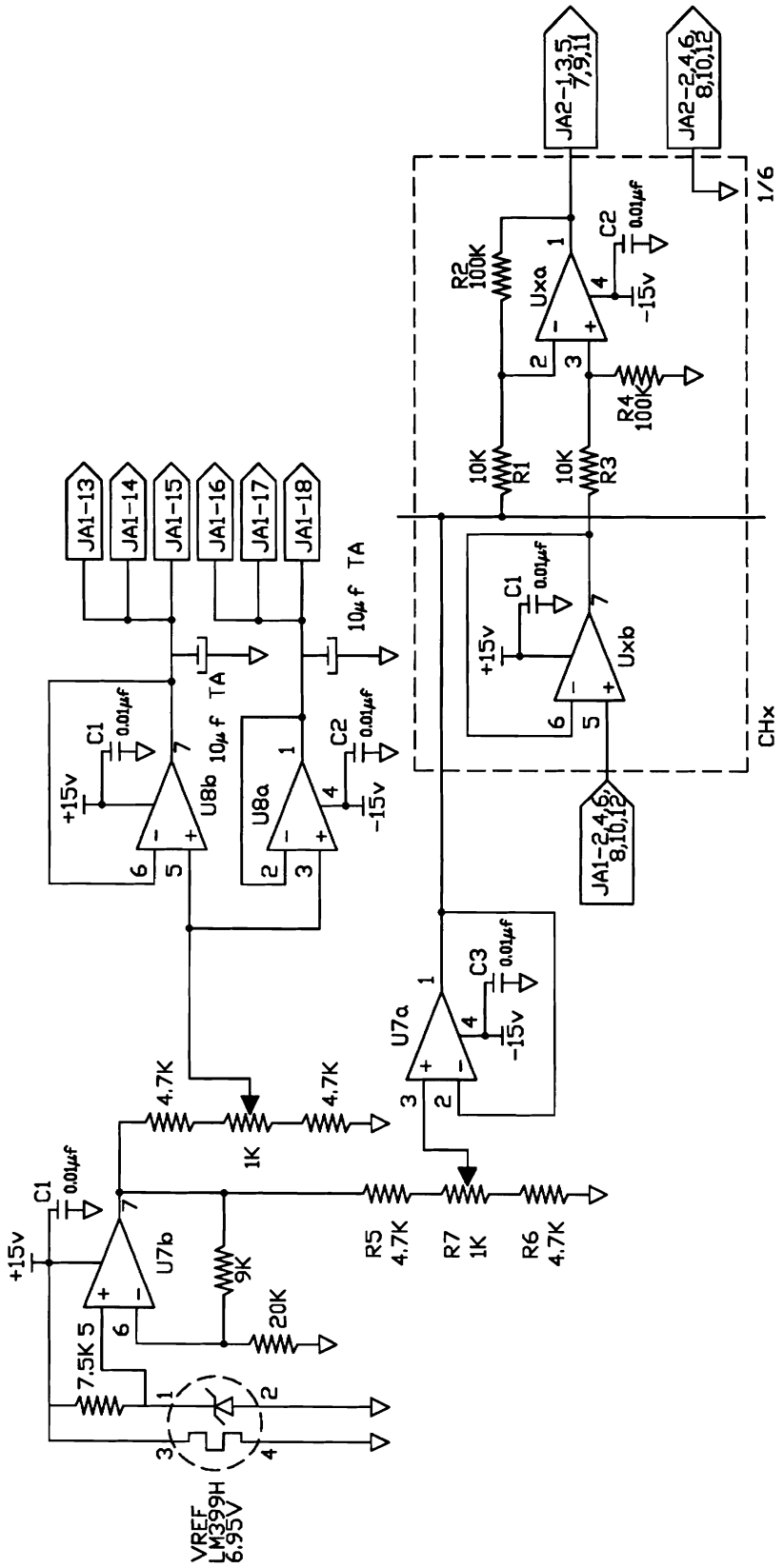

Figure 25: Signal Conditioning Board

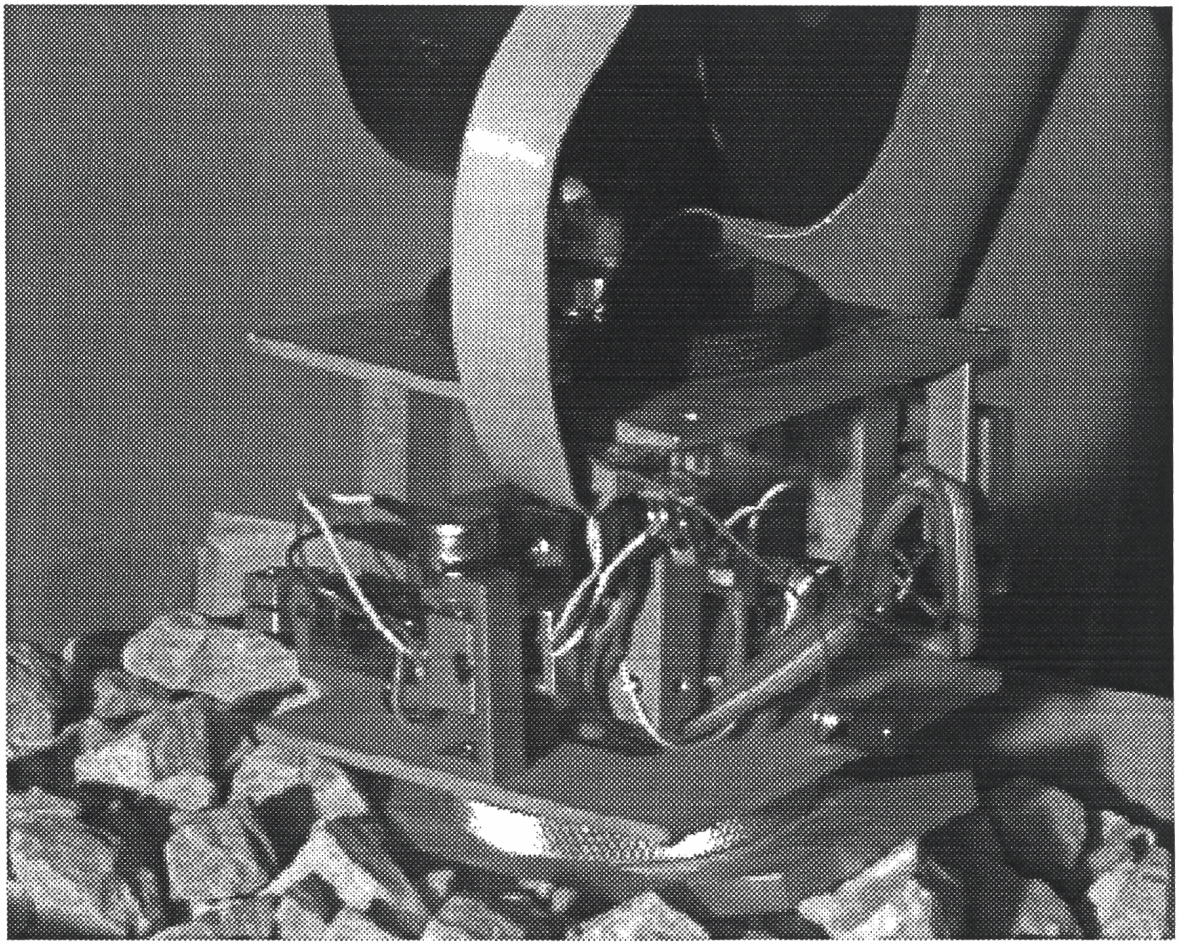

Figure 26: Exploration and locomotion application (courtesy, P. Sinha)

7 Conclusion and Future Work

The wrist outlined here is currently in use in the GRASP lab. Projects using the wrist include "Teleprogramming: Towards Delay-Invariant Remote Manipulation" [2], "Robotic Exploration of Surfaces with a Compliant Wrist Sensor" [6], and "Simlifying Tool Usage in Teleoperative Tasks" [4]. Figure 26 illustrates the previous wrist design in use exploring the environment[4]. Figure 27 shows the robot/wrist holding an impact wrench, undoing a bolt. Figure 28 shows the Penn Hand attached to the wrist, using artificial intelligence to learn object grasping techniques. The wrist has been shown to be a useful force/torque sensor for hybrid position/force control implementations[3].

Two major improvements to the wrist would improve the usefulness and accuracy. First, determination of the complete 6x6 stiffness matrix for the wrist would both improve the accuracy of force control algorithms and characterize the effects of the coupling of orthogonal forces. This would lead to more accurate control. Second, the accuracy of the sensing linkage could be improved by using resolvers instead of potentiometers at the linkage joints, or possibly substituting a parallel sensing linkage structure using LVDTs as position transducers.

[4]Note that application pictures shown in this section are actual implementations of the previous wrist design

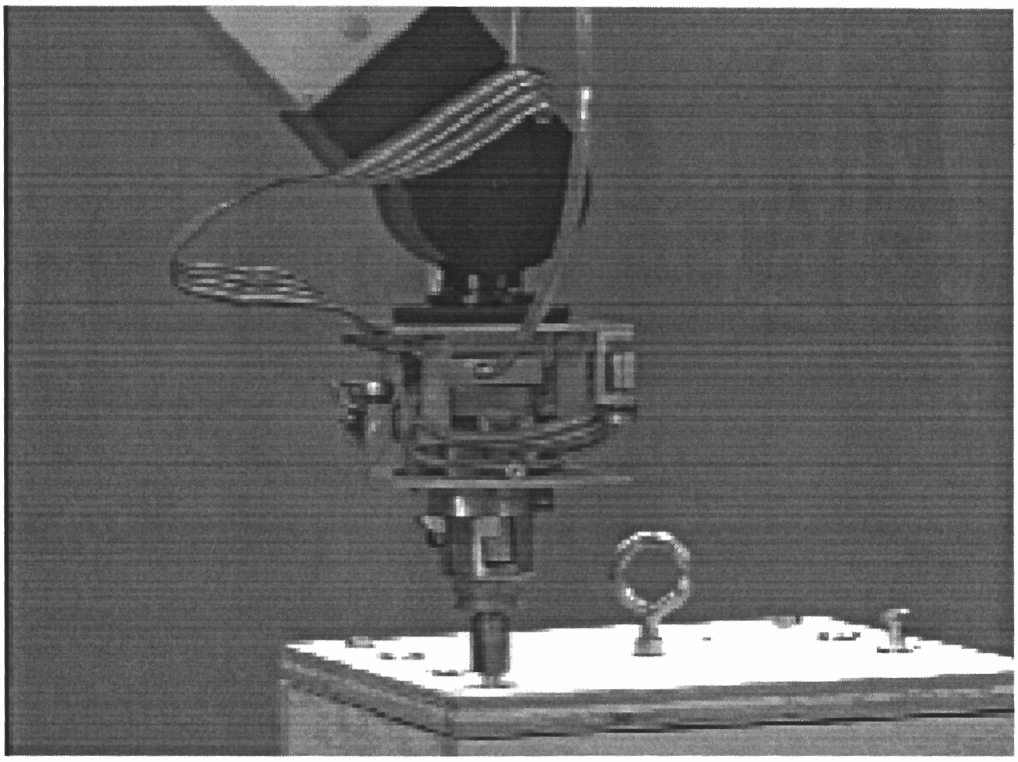

Figure 27: Impact wrench attached to wrist

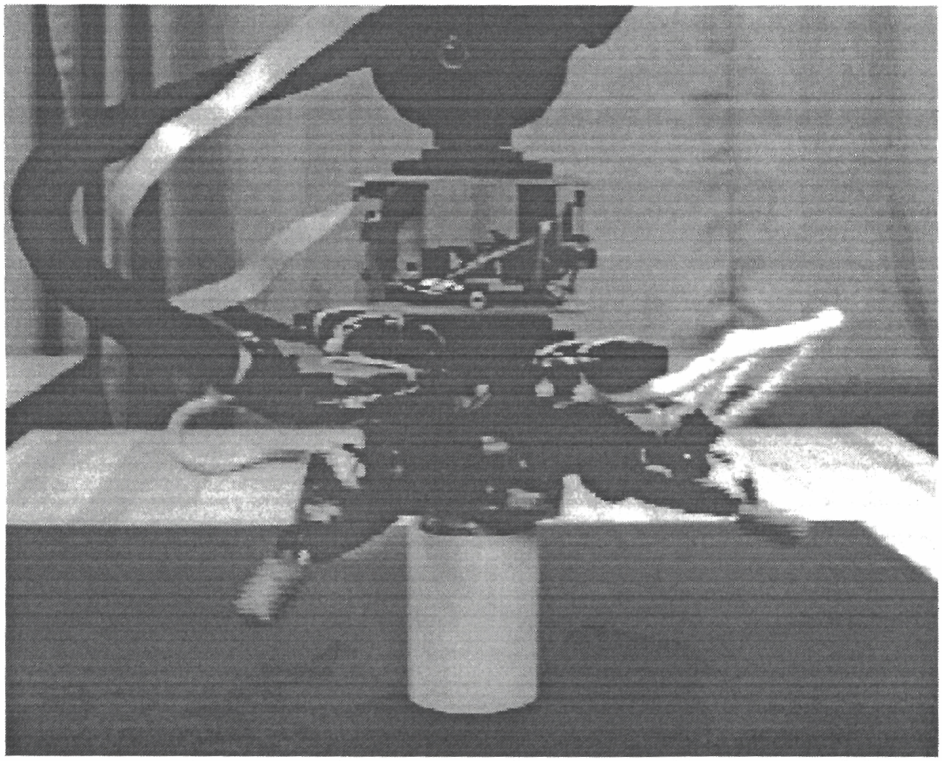

Figure 28: Penn Hand attached to wrist (courtesy, M. Salganicoff)

References

[1] *Vibration and Shock Mount Handbook.* Stock Drive Products, New Hyde Park, NY, 1984. Product Catalog 814.

[2] Janez Funda. *Teleprogramming: Towards Delay-Invariant Remote Manipulation.* PhD thesis, University of Pennsylvania, 1991.

[3] Thomas S. Lindsay. *Teleprogramming: Remote Site Robot Task Execution.* PhD thesis, University of Pennsylvania, 1992.

[4] Thomas S. Lindsay and Richard P. Paul. Simplifying tool usage in teleoperative tasks. In *SPIE Telemanipulator Technology*, November 1992.

[5] Randall K. Roberts, R. P. Paul, and Benjamin M. Hillberry. The effect of wrist force sensor stiffness on the control of robot manipulators. In *Proceedings of the IEEE International Conference on Robotics and Automation*, pages 269–274, April 1985.

[6] P.R. Sinha, Y. Xu, R.K. Bajcsy, and R.P. Paul. Robotic Exploration of Surfaces using a Compliant Wrist Sensor. *International Journal of Robotics Research*, 12(1), February 1993. To appear.

[7] Richard Volpe and Pradeep Khosla. Experimental verification of a strategy for impact control. In *Proceedings of the IEEE International Conference on Robotics and Automation*, pages 1854–1860, 1991.

[8] Yangsheng Xu. *Compliant wrist design and hybrid position/force control of robot manipulators.* PhD thesis, University of Pennsylvania, 1989.